

# Effects of ablative and non-ablative laser shock peening on AA7075-T651 corrosion and fatigue performance

A.G. Sanchez, Mitchell Leering, Daniel Glaser, D. Furfari, M. E. Fitzpatrick, J. A. Wharton, and P. A. S. Reed

**Final Published Version deposited by Coventry University's Repository**

**Original citation & hyperlink:**

Sanchez, A.G., Leering, M., Glaser, D., Furfari, D., Fitzpatrick, M.E., Wharton, J.A. and Reed, P.A.S., 2021. Effects of ablative and non-ablative laser shock peening on AA7075-T651 corrosion and fatigue performance. *Materials Science and Technology*

<https://doi.org/10.1080/02670836.2021.1972272>

DOI [10.1080/02670836.2021.1972272](https://doi.org/10.1080/02670836.2021.1972272)

ISSN 0267-0836

ESSN 1743-2847



Publisher: Taylor and Francis

© 2021 The Author(s). Published by Informa UK Limited, trading as Taylor & Francis Group

This is an Open Access article distributed under the terms of the Creative Commons Attribution License

(<http://creativecommons.org/licenses/by/4.0/>), which permits unrestricted use, distribution, and reproduction in any medium, provided the original work is properly cited.

## Effects of ablative and non-ablative laser shock peening on AA7075-T651 corrosion and fatigue performance

A. G. Sanchez <sup>a,b</sup>, M. Leering<sup>c</sup>, D. Glaser<sup>d</sup>, D. Furfari<sup>e</sup>, M. E. Fitzpatrick <sup>c</sup>, J. A. Wharton<sup>b</sup> and P. A. S. Reed<sup>a</sup>

<sup>a</sup>Materials Research Group, Faculty of Engineering and Physical Sciences, University of Southampton, Southampton, UK; <sup>b</sup>National Centre for Advanced Tribology at Southampton, Faculty of Engineering and Physical Sciences, University of Southampton, Southampton, UK;

<sup>c</sup>Faculty of Engineering, Environment, and Computing, Coventry University, Coventry, UK; <sup>d</sup>National Laser Centre, Council for Scientific and Industrial Research, Pretoria, South Africa; <sup>e</sup>Airbus Operations GmbH, Hamburg, Germany

### ABSTRACT

The fatigue performance from pre-corroded pits was studied in laser-shock-peened AA7075-T651 with and without a protective ablation-layer. Surface and microstructural characterisation showed laser-shock-peening generated residual stresses up to  $-400\text{MPa}$ , limited hardness and moderate surface roughness increase. The laser-shock-peened specimens were exposed to 3.5 wt-% sodium chloride solution for different levels of galvanostatic control. The compressive residual stresses did not significantly affect corrosion behaviour, or corrosion pit morphology. Laser-shock-peening-induced surface roughness had the most detrimental impact on corrosion performance. Fatigue testing of pre-corroded AA7075-T651 showed pits act as stress concentrations. Cracks initiated shortly after dynamic loading, reducing fatigue life by 50%. Laser-shock-peening increased fatigue life by 400% compared to corroded-untreated AA7075-T651, due to residual stresses effectively counteracting stress concentrations produced by pits.

### Highlights

- Pre-corroded laser-peened (LSP and LSPwC) AA7075-T651 fatigue performance is investigated.
- XRD and incremental hole drilling show deeper compressive residual stresses for LSPwC compared to LSP.
- Electrochemical tests show no significant changes in corrosion behaviour after laser peening.
- Fatigue testing and fractography show compressive residual stresses effectively counteract stress concentrations at pits.

### ARTICLE HISTORY

Received 24 March 2021  
Revised 5 August 2021  
Accepted 20 August 2021

### KEYWORDS

Laser shock peening; pre-corroded; corrosion performance; fatigue performance; material characterisation; aluminium alloy; ablation; compressive residual stress

## Introduction

Laser shock peening, commonly referred to as LSP, is a mechanical surface treatment similar to shot peening, that imparts beneficial compressive residual stresses to a metallic surface up to a depth of several millimetres. It can also cause grain refinement, generation of high-density dislocations, and small amounts of twinning [1,2]. Laser shock peening uses high-power laser pulses to ionise the surface, forming a plasma that is confined within a transparent inertial confinement medium (typically water). The confined plasma generates high pressure (of the order of GPa), transmitting shock waves into the metal surface, producing a constrained localised surface and subsurface plastic deformation, and thus compressive residual stresses [3–5]. An ablative, sacrificial coating, either black tape or aluminium foil, is often used as a thermo-protective overlay to preserve the surface integrity of the target.

Alternatively, laser peening can be performed without an ablative coating (commonly referred to as LSPwC), which was originally developed for underwater laser peening to prevent stress corrosion cracking in nuclear power plant, where access to apply an ablative coating is not possible [6]. In LSPwC a thin layer of the material's surface is ablated, generating the plasma shock wave to impart compressive residual stresses. Advantages of LSPwC versus the standard laser shock peening with ablative layer (hereinafter called LSP) are the ability to employ compact and commercially available lasers, deliver laser pulses through flexible optical fibre, ability to irradiate laser pulses to water-immersed objects and a reduction in peening-processing time [6].

The aerospace industry is using laser shock peening more extensively, and in some instances in preference to shot peening. Indeed, laser shock peening is seen as a promising method for improving fatigue

**CONTACT** A. G. Sanchez  agsa1m17@soton.ac.uk

life of aerospace aluminium components [3]. There are several benefits to choosing laser shock peening over shot peening, including greater accuracy and precision [3,7,8], greater depth and magnitude of the subsurface compressive residual stresses [3,7,9,10]; beneficial decrease in detrimental surface modification; and fatigue life improvements [3,11].

Laser-peening effectiveness on fatigue life depends on the combination of laser parameters chosen in terms of the level of compressive residual stresses [12–14,8,11,15–17], the surface roughness [11,18–20] and the surface hardness [9–11,19,21–23]. Key laser-peening parameters can also change the effectiveness of the treatment on fatigue performance in treated 2XXX alloys [12–14] and 7XXX alloys [16,7,11,20]. Recently, Sanchez et al. [24] reported an LSP treatment on AA7075-T651 that maximised residual stresses, whilst minimising surface roughness. The LSP altered the fatigue crack initiation mechanism, and significantly delayed both initiation and propagation. However, the LSP-generated small pits, up to 12  $\mu\text{m}$  in diameter, which have been previously attributed to localised air compression under the laser shockwave [25,26]. The Sanchez et al. [24] study found in most instances the crack initiation mechanism and fatigue life extension were affected by the presence of the pits induced by the LSP treatment, which act as stress raisers and markedly lowered fatigue crack initiation time. Since these small LSP mechanical pits can hinder fatigue performance, and considering the susceptibility and exposure of aluminium alloys to corrosive environments in the aerospace industry [27], it raises the question of how corrosion pits may develop and affect fatigue performance in a laser-peened material (with and without coating). Specifically, how do LSP (or LSPwC) residual stresses and the modified surface affect electrochemical behaviour; how does laser shock peening promote or diminish corrosion pit formation, and how do fatigue cracks initiate and propagate from pre-existing corrosion features within a peening-induced residual stress field.

It has been established that compressive residual stresses are beneficial in retarding corrosion phenomena that require mechanical stimuli, such as stress corrosion cracking [28–35] and corrosion fatigue [28,36–40]. Specifically, for LSPwC, studies report compressive residual stresses can improve corrosion performance. For example, studies on an LSP aerospace alloy [41,42] and aluminium–silicon alloys [22] show improvement in pit numbers and size after laser peening, and a decrease in corrosion current density, and show how increased power density will increase surface roughness, in most cases promoting higher corrosion current density. In the case of AA7075, one study [43] shows a small (50 mV) ennoblement in open-circuit potential after shot peening. Another study reported a more varied performance: LSPwC

AA7075-T651 had a slight increase in corrosion current density but a decrease in number of pits compared to the baseline [36]. Whilst these studies clearly show LSPwC-induced roughness to be detrimental to corrosion performance, the link between LSPwC-generated compressive residual stresses and oxide-formation, on corrosion performance improvement, is more tenuous.

In this study, the effects of LSP (ablative laser peening) and LSPwC (non-ablative) treatments on the corrosion performance and fatigue performance of corroded AA7075-T651 are investigated. The objectives are to understand to what extent the laser-shock-peening-generated residual stresses and the modified surface (microstructure, hardness and roughness) influence the AA7075-T651 electrochemical properties and corrosion performance. Additionally, to understand if the formation of corrosion pits is hindered or encouraged by LSP, or LSPwC, treatment. Finally, to investigate how pre-corroded pit features can affect the fatigue performance, and crack initiation mechanisms, previously seen for laser-shock-peened AA7075-T651 [24].

## Methodology

### Materials and LSP surface treatment

The test material was sourced from an AA7075-T651 (UNS A97075) plate, with mechanical properties: a tensile strength of 572 MPa, yield strength of 503 MPa, approximate hardness of HV175 and fracture toughness of 20–29  $\text{MPa}\sqrt{\text{m}}$  depending on the microstructural plane loaded [44]. The major alloying elements are zinc, magnesium and copper. The T651 temper condition indicates solution heat treatment, artificial ageing and stretching (to relieve internal residual stresses). All test samples were sectioned from the AA7075-T651 plate, with the top surface (the surface tested) in the L-LT plane (see Figure 1). Three surface conditions were tested: untreated AA7075 (baseline), LSP (laser shock peening with ablative layer) and LSPwC (laser shock peening without ablative layer followed by a light mechanical grind to remove the oxide layer to improve fatigue life, see Section Laser-shock-peening treatment). LSP and LSPwC surface treatments were applied to two sample types: identified as A and B. Type A are fatigue bend bars with dimensions as identified in Figure 1, where the LSP-induced compressive residual stresses are considered to remain intact when subsequently tested. Type B are small bars (5 mm  $\times$  5 mm  $\times$  35 mm) machined from a large laser-peened block, as shown in Figure 1. It is well-known that removing a volume from a region containing residual stresses will relieve these stresses within the discrete section, and the smaller the sample removed from the original laser-peened material the greater the

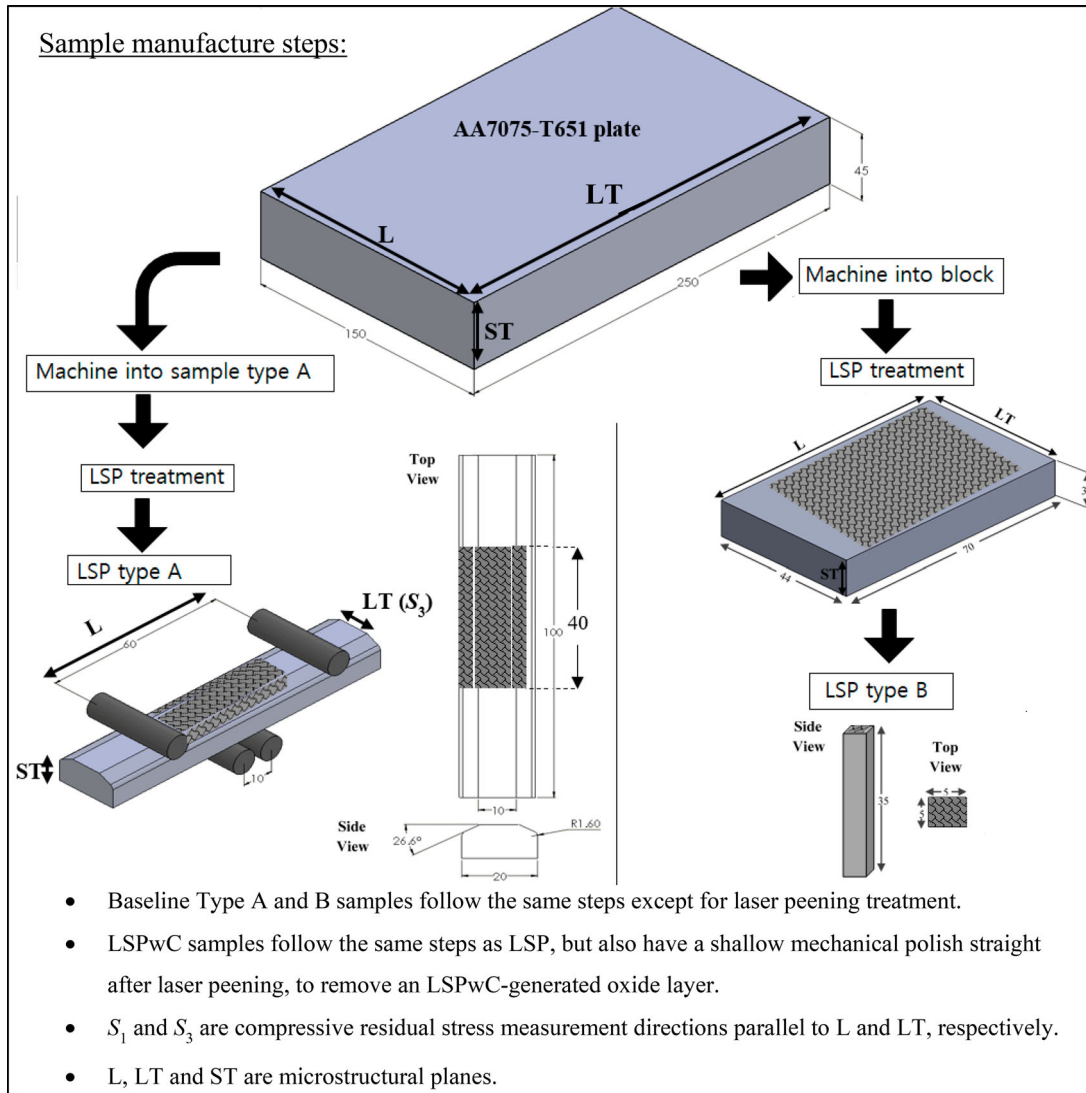


**Figure 1.** Sample manufacturing steps (Type A and B).

stress relief [45]. Thus, Type B are assumed to have negligible residual stress.

### Laser-shock-peening treatment

Ablative laser shock peening (LSP) and non-ablative laser shock peening (LSPwC) were performed at the Council for Scientific Research and Innovation (CSIR), South Africa. A Thales SAGA pulsed Nd:YAG laser was used and the peening parameters are shown in Table 1. As laser peening in industry is performed to improve fatigue performance, LSPwC had one additional step involving the mechanical removal of a thin oxide layer present to greatly improve the surface compressive residual stress. The oxide removal was performed at the CSIR, using a deburring brush (a very fine Scotch-Brite™ ‘red’ pad), a method used in industry. Further removal details can be found in Niknam and Songmene [46]. For Type A, the top surface and the chamfer surfaces were peened to avoid crack formation outside the top surface, as shown in Figure 1. Type B were cut from peened blocks, as seen in Figure 1. The

**Table 1.** Laser-peening parameters.

Parameter	Value
Power density/GW cm <sup>-2</sup>	4
Wavelength/nm	532
Spot shape	Circular
Dimension/mm	1.5 dia.
Spot offset/%	0.225
Spot overlap/%	166.7 spots cm <sup>-2</sup> (≈ 48.4%)
Energy/mJ	364
Sacrificial coating	Black vinyl tape (LSP)/No coating (LSPwC)

same peening parameters were used for Type A and B samples.

### Surface and microstructural characterisation

A Talysurf contact profilometer with a vertical resolution of 4 nm was used to measure roughness testing (ISO4287 standard). Micro-hardness measurements used an FM-300 Microhardness Tester machine, with a 0.5 kg-f load and 30 s hold time. Eight to 15 readings were taken from each test sample. An Alicona

InfiniteFocus™ focus variation microscope, at  $\times 20$  magnification and 150 nm vertical resolution, was used to assess the surface. A JEOL JSM-6500F scanning electron microscope (SEM) for secondary electron imaging (SEI) and backscatter electron imaging (BEI), including energy-dispersive X-ray spectroscopy (EDS) was used to qualitatively identify second-phase intermetallics. Electron backscatter diffraction (EBSD) was used to analyse microstructures after laser shock peening. The voltages used for SEI imaging, BEI imaging and EDS, and EBSD were 10, 15 and 20 keV, respectively. The EBSD samples were mechanically polished to a 3  $\mu\text{m}$  surface finish with diamond suspension followed by electropolishing (2:1 methanol and nitric acid, 25–30 V, 25–35°C, 2–5 s). EBSD data was imported into Matlab R2018a and re-analysed using MTEX algorithm [47] to create a map of kernel average misorientation (KAM) versus distance from the LSP and LSPwC surfaces. For more information on EBSD method details see Sanchez et al. [24].

### Residual stress analysis

X-ray Diffraction (XRD) and incremental centre hole drilling were used in a complementary manner, to assess the residual stresses present in the LSP and LSPwC samples at and below the surface [48]. The XRD measurements were made with a Stresstech Xstress diffractometer located on an articulated robotic arm, utilising the  $d\text{-sin}^2\psi$  technique to determine the stress. A chromium X-ray source was used with a 1 mm diameter collimator and counting time of 20 s at each of the 14 tilt locations evenly spaced between  $-45/45^\circ$ . The  $0^\circ$  and  $90^\circ$  measurement angles were aligned with the longitudinal ( $S_1$ ) and transverse ( $S_3$ ) directions of the samples (see Figure 1).

The incremental hole-drilling measurements were made with a Stresscraft three-axis drilling device. Measurements were made at 23 surface-biased (smaller increments near the surface) incremental depths using an orbital drilling motion. The measurements were taken in the centre of the laser-peened region on the bend bar sample. Strain readings were taken to a depth of 1.024 mm from the surface in the longitudinal ( $S_1$ ) and transverse ( $S_3$ ) directions of the samples (see Figure 1). Further details of the XRD and hole-drilling methodology are given in Sanchez et al. [24].

### Corrosion testing

To characterise the electrochemical properties of the AA7075-T651 laser-peened surface the remaining sample surface was masked using a mixture of beeswax and colophony resin (3:1 ratio), leaving only 25 mm<sup>2</sup> unmasked. All electrochemical tests were performed at ambient temperature and atmospheric conditions.

After corrosion exposure, the samples were ultrasonically cleaned in ethanol (45 min at 50°C) to remove soluble corrosion products.

Electrochemical measurements were carried out in a Faraday cage, in a single compartment three-electrode cell with a silver/silver chloride (Ag/AgCl) reference electrode, a graphite counter electrode, and a 3.5 wt-% NaCl test solution. A VMP3 Biologic VSP multi-channel potentiostat and EC-Lab v11.10 software were used to perform the tests and interpret data.

The electrochemical tests are 30 min and 24 h open-circuit potential. Additionally, a small number of samples were exposed to 72 h OCP for subsequent microscopy analysis of corrosion feature initiation mechanisms. Other electrochemical tests performed were potentiodynamic polarisation ( $-0.250\text{ V} < E_{\text{corr}} < +0.350\text{ V}$  with a  $0.2\text{ mV s}^{-1}$  sweep rate), and galvanostatic control ( $2\text{ mA cm}^{-2}$  for 2 h and  $0.157\text{ mA cm}^{-2}$  for 24 h, high and low galvanostatic control, respectively). The two galvanostatic exposures aim to capture corrosion behaviour at two different regimes. The total charge was the same for both low and high galvanostatic control (144 C). An Alicona™ variable focus microscope was used to study the surface topography after corrosion testing. Images of a corroded area were assessed using Fiji image software [49], where the following steps are followed to quantify the pit features: rotate, crop, colour threshold, eight-bit image, threshold and analyse particles. Also, Origin(pro) 2020 was used to evaluate corrosion pit area fractions (the sum of all corroded surfaces over the measurement area) and pit density (pits per mm<sup>2</sup>).

### Fatigue testing

A servo-hydraulic Instron machine was used for four-point bend testing. The four-point bend test was performed at a frequency of 20 Hz and a load ratio of 0.1. The load setup is shown in Figure 1. The fatigue samples area identified in Table 2.

Prior to fatigue testing, all corroded baseline and laser-peened samples were exposed to the high galvanostatic control ( $2\text{ mA cm}^{-2}$  for 2 h) to generate corrosion features at ambient conditions. After corrosion exposure, the samples were ultrasonically cleaned in ethanol (45 min at 50°C) to remove soluble corrosion products. All pits bigger than 10  $\mu\text{m}$  are assumed to

**Table 2.** Condition of fatigue test samples.

Sample condition	Details
Baseline	Untreated [24]
LSP	Ablative LSP treatment [24]
LSPwC	non-Ablative LSP treatment
Base + Corr	Untreated + corrosion exposure
LSP + Corr	Ablative LSP treatment + corrosion exposure
LSPwC + Corr	non-Ablative LSP treatment + corrosion exposure



be corrosion-generated (not laser-peening-generated mechanical pits) and are characterised as such.

Two methods were used for crack propagation capture: (i) the replica method for baseline samples only; and (ii) the beach marking method for all laser-peened and corroded samples. The replica method consists of using ready-made replica material Struers F5. Cracks were measured and used to calculate sample's crack growth rate  $da/dN$  as a function of stress intensity factor ( $\Delta K$ ).

For laser-peened samples and all corroded samples, the replica method was not effective in monitoring crack behaviour due to subsurface crack initiation and growth. In this case, the beach marking method was used. Instron wave matrix was used to set up a regime where the load ratio was varied from  $R = 0.1$  to  $R = 0.5$ . The variation in load ratio was performed by increasing the minimum load, keeping the maximum load, and therefore  $K_{max}$ , constant during the whole test. The number of cycles for each load ratio was chosen based on expected total life and experimental trial. For the ' $R = 0.1$  to  $R = 0.5$ ' tests, fatigue life is presented as an estimate with error bars. The estimated life ( $N_{Total}$ ) is equal to the cycles under ' $R = 0.1$ ' ( $N_{R=0.1}$ ) plus a third of the cycles under ' $R = 0.5$ ' ( $N_{R=0.5}$ ).

$$N_{Total} = N_{R=0.1} + \left[ \frac{N_{R=0.5}}{3} \right] \quad (1)$$

This is based on the Walker equation for AA7075-T651 by Dowling et al. [50], and a set of AA7075-T651 uniaxial data [51], to estimate fatigue life for different load ratios. Error bars are also presented to show the minimum fatigue life ( $N_{R=0.1}$ ) and the maximum fatigue life ( $N_{R=0.1} + N_{R=0.5}$ ) [24].

Optical microscopy and scanning electron microscopy were used to analyse fracture surfaces of fatigue samples, for both baseline, LSP and LSPwC samples. SEM microscopy (10–15 keV), Fiji image processing [49], and fatigue data (number of cycles and load ratio) are used to measure crack size and calculate crack growth versus  $\Delta K$ .

## Results

### Material characterisation

Figure 2 shows a three-dimensional representation of the AA7075-T651 microstructure. The microstructural planes are L-LT, L-ST and LT-ST. The L direction is orientated along the rolling direction, which results in grains that are anisotropic and characteristically elongated in shape. The dark features (between 1 and 10  $\mu\text{m}$  in size) are coarse intermetallics. SEM-EDS suggest these are mostly  $\text{Al}_7\text{Cu}_2\text{Fe}$  and  $\text{Al}_{23}\text{Fe}_4\text{Cu}$ , and occasionally  $\text{Mg}_2\text{Si}$ . Line intercept measurements according to the ASTM-E112-12 planimetric method give an

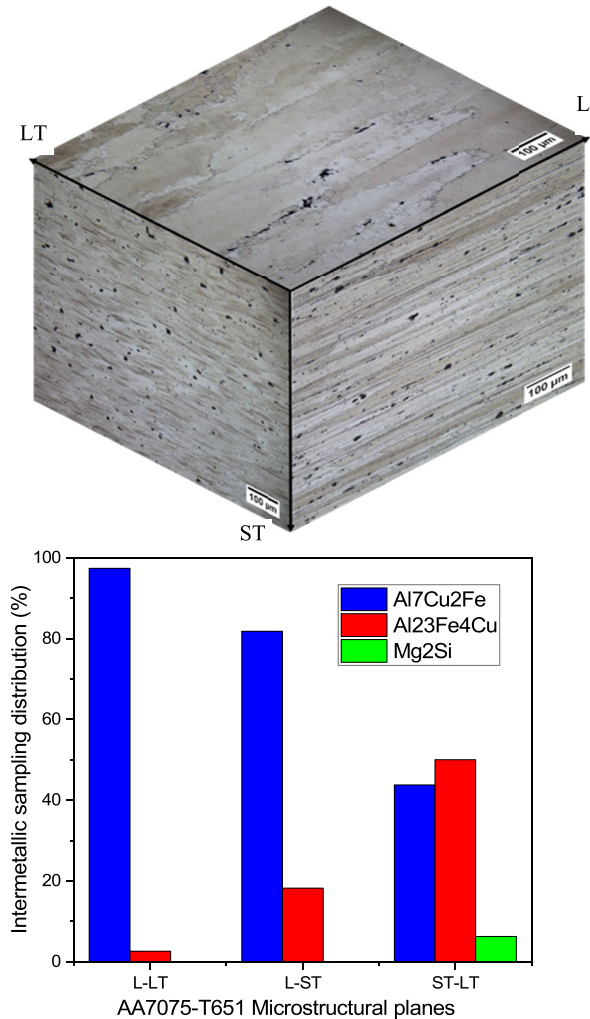


**Figure 2.** (a) Three-dimensional representation of AA7075-T651 microstructural planes and (b) intermetallic distribution from SEM-EDS random sampling.

**Table 3.** AA7075-T651 average grain size.

Average	L/ $\mu\text{m}$	LT/ $\mu\text{m}$	ST/ $\mu\text{m}$
From L-LT plane	141	66.7	
From LT-ST plane		53.2	14.8
From L-ST plane	312		14.0
Final	227	66.7	14.4

Comments on grain size: 100s microns (L), High 10s to low 100s microns (LT), 10s microns (ST).  
Note: Line intercept method according to the ASTM-E112-12 planimetric method.

average of  $227 \mu\text{m} \times 67 \mu\text{m} \times 14 \mu\text{m}$  for the L, LT and ST directions, respectively (Table 3).

### Residual stress

The LSP centre hole-drilling data in Figure 3 shows that longitudinal ( $S_1$ ) and transverse direction ( $S_3$ ) compressive residual stresses achieved a maximum of approximately  $-400 \text{ MPa}$  subsurface. XRD measurements show surface residual stress of up to  $-330 \text{ MPa}$ . From a maximum of  $-400 \text{ MPa}$  the residual stresses progressively decrease to  $-50 \text{ MPa}$ , at 1 mm subsurface. For LSPwC, XRD measurements of residual stress

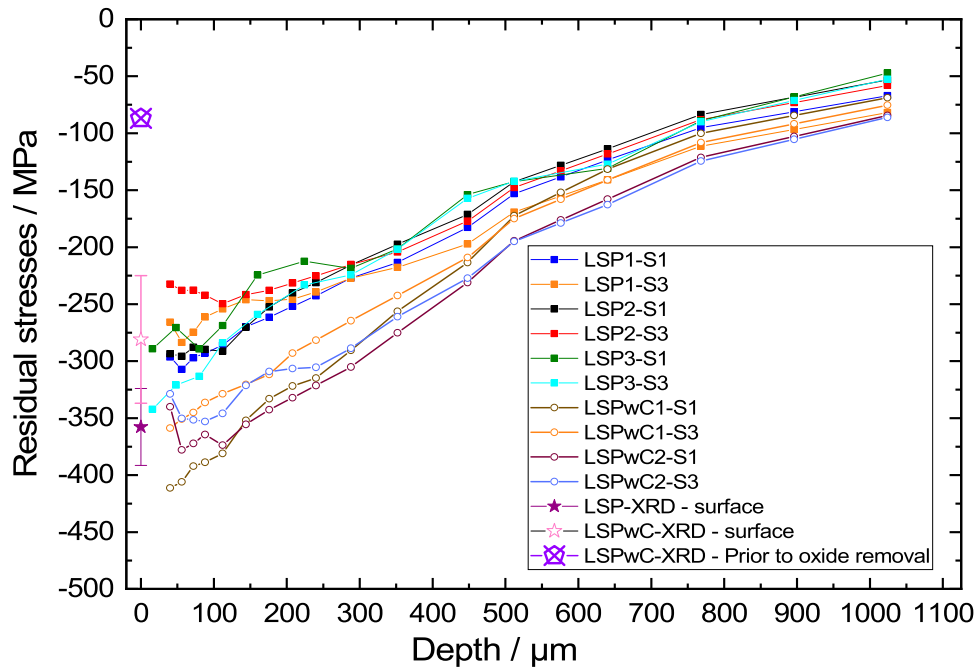


**Figure 3.** Centre hole-drilling and XRD data for LSP and LSPwC samples.  $S_1$  in the longitudinal direction,  $S_3$  in the transverse direction.

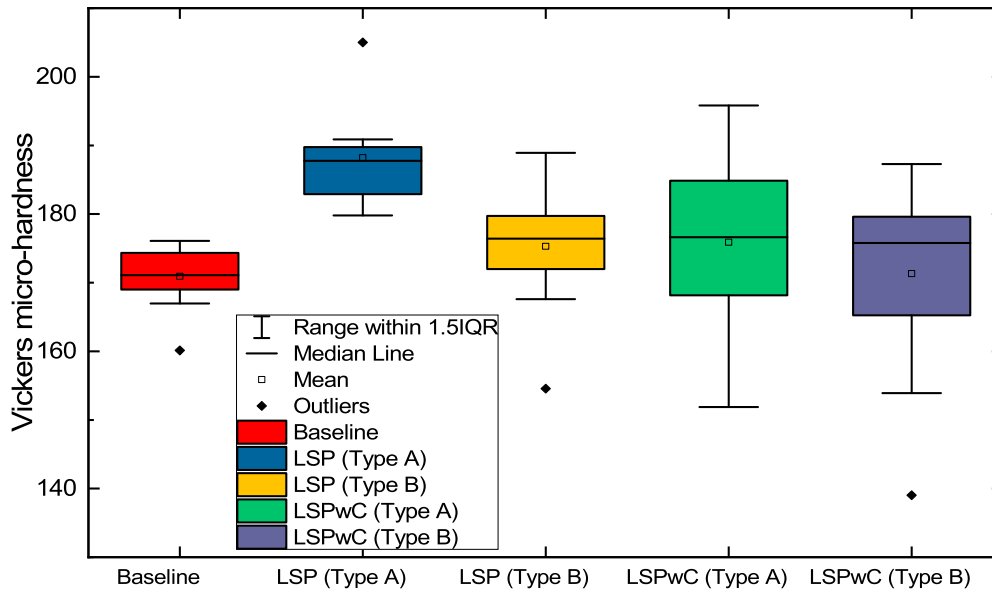


**Figure 4.** Vickers micro-hardness measurements of baseline, LSP and LSPwC Type A and B samples.

before oxide layer removal give  $-85$  MPa. After oxide removal (see Section Laser-shock-peening treatment) the maximum compressive residual stress at the surface is approximately  $-275$  MPa. The centre hole-drilling data for LSPwC in Figure 3 show compressive residual stresses of up to  $-405$  MPa in the first  $56$   $\mu\text{m}$  below the surface, progressively decreasing away from the surface. The measurements suggest LSPwC has higher compressive residual stresses than LSP, by up to  $100$  MPa in the first  $800$   $\mu\text{m}$ , with the difference being more pronounced in the first  $400$   $\mu\text{m}$ .

### Surface and near-surface modification

According to Figure 4, the LSP Type A average micro-hardness is  $188$  Hv, an  $11\%$  increase compared to the

baseline average hardness of  $170$  Hv. Average hardness for LSP Type B that is subject to residual stresses relief is  $175$  Hv. The LSPwC Type A and B average hardness are  $176$  and  $171$  Hv, respectively. Unlike LSP Type A and baseline, the interquartile range of LSPwC Type A is larger, thus indicating greater variability.

The roughness data, in Table 4, show a doubling (LSP) or tripling (LSPwC) of  $R_z$ ,  $R_t$  values; and tripling (LSP) or quadrupling (LSPwC) of  $R_a$ ,  $R_q$  values. There has been an increase in roughness from baseline to LSP, and even higher for LSPwC. Nevertheless, generally these values are of the same order of magnitude. However, Figure 5 shows LSPwC has a clear wavy surface profile from the laser-peening ripple features. This ripple effect is not as pronounced in LSP.

**Table 4.** Average roughness measurements for baseline, LSP and LSPwC (all Type A samples).

Roughness parameter	Baseline (1 $\mu\text{m}$ )	Baseline (1200 SiC grind)	LSP	LSPwC
$R_a/\mu\text{m}$	0.04	0.23	0.76	1.03
$R_q/\mu\text{m}$	0.04	0.29	0.90	1.24
$R_z/\mu\text{m}$	0.17	1.62	3.69	5.28
$R_t/\mu\text{m}$	0.25	2.64	5.52	7.94
$R_{sk}$	0.06	-0.10	-0.11	0.03

### Grain microstructure analysis

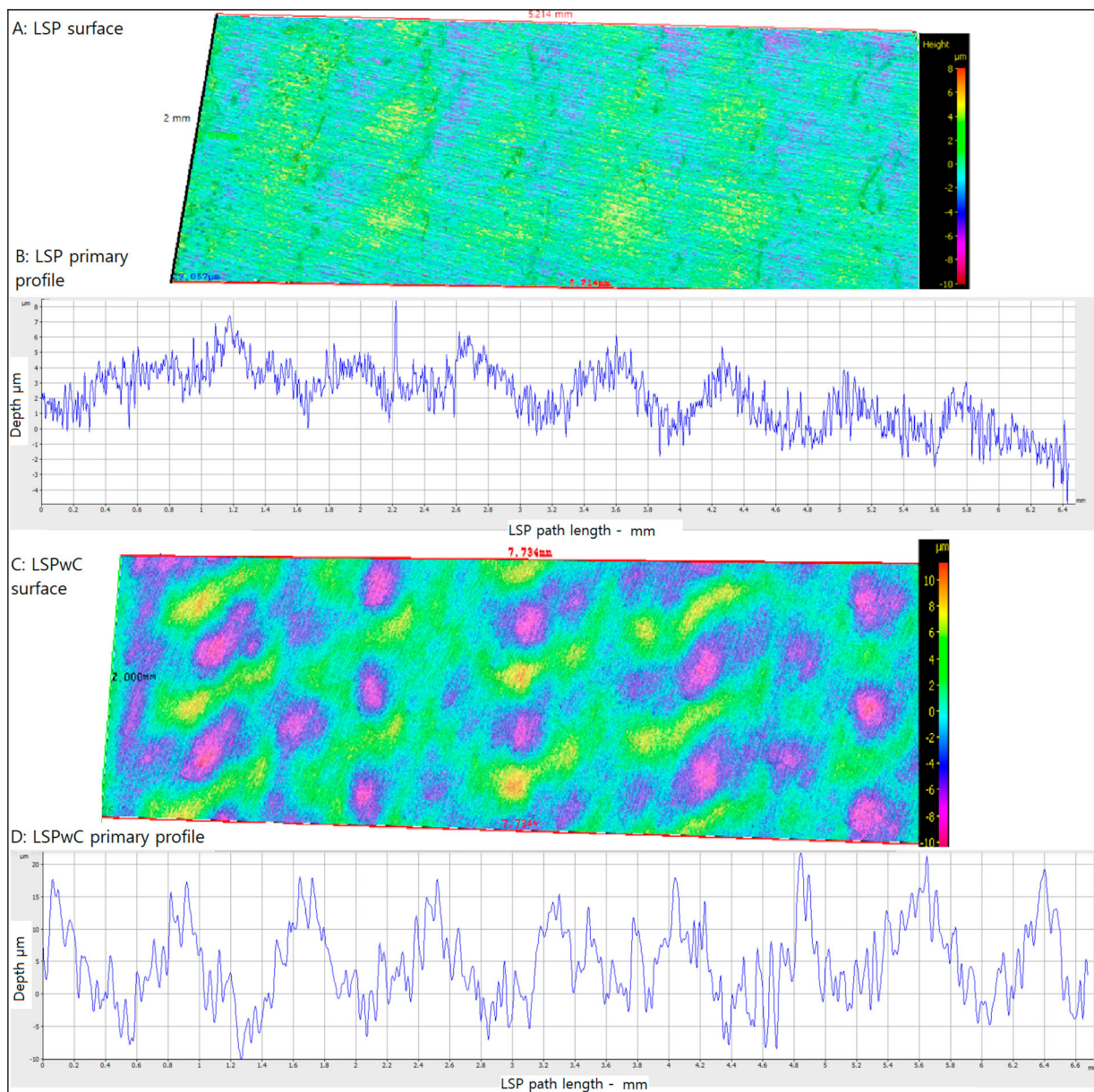
EBSDF was not able to capture grain data for the surface and the first 20  $\mu\text{m}$  below the surface due to the limitations of EBSDF indexing on highly deformed surfaces [52,53]. Thus, the expected surface and near-surface grain refinement from laser peening [1,2] could not be investigated quantitatively.

KAM data for the LSP cross-section (Figure 6) clearly show higher grain deformation near the surface (above  $1.5^\circ$  closest to surface), progressively decreasing away from the surface to a stable  $0.5^\circ$ – $1^\circ$ . This suggests, that as demonstrated by the EBSDF recrystallization maps presented previously [24], LSP causes grain deformation, and is highest at the top surface, progressively decreasing away from the surface.

### Corrosion performance

#### Open-circuit potential

Figure 7 shows the Open-circuit potential (OCP) measurements for the baseline, LSP and LSPwC in Type A (Figure 7(A,C)) and Type B (Figure 7(B,D)) samples. As previously noted, some (if not all) residual stress relief is expected for Type B. Initial OCP for the baseline was similar for the three replicates, between  $-0.730$

**Figure 5.** LSP and LSPwC surfaces and profiles.



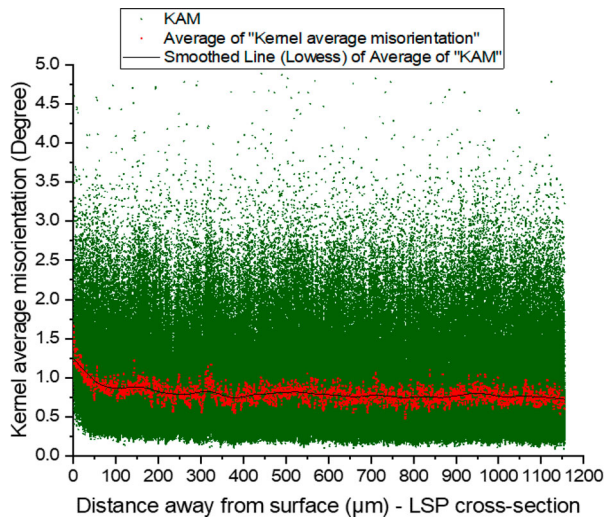


**Figure 6.** Kernel average misorientation (KAM) data, average and smooth line of LSP cross-section (LT-TS microstructural plane), distance away from surface from left to right, up to 1.15 mm subsurface. Taken from Sanchez et al. (2021).

and  $-0.740$  V. In contrast, initially for LSP and LSPwC the corrosion potentials varied between  $-0.730$  and  $-0.690$  V, leading to a more transient response caused by the peened surface. Nevertheless, overall during the initial 30 min (Figure 7(A,B)) the OCPs for all surfaces were relatively similar (within 30 mV); whereas, after 24 h (Figure 7(C,D)) the OCPs for all peened surfaces tend to decrease to between  $-0.775$  and  $-0.800$  V, unlike the baseline which stayed relatively uniform.

### Potentiodynamic polarisation

Figure 8(A) shows the potentiodynamic polarisations for untreated AA7075 (baseline), LSP and LSPwC Type A and B. In terms of corrosion potential, the baseline are similar, between  $-0.750$  and  $-0.735$  V; whilst LSP values are generally more variable. LSP Type B are in the same range as baseline. In contrast, LSP Type A appear to have more varied free corrosion potential, and are generally nobler than the baseline, by no more than 40 mV. The anodic curves for all samples are similar, suggesting no particular difference in the anodic corrosion kinetics between baseline and LSP. Additionally, the cathodic slopes of the LSP Type B are a magnitude lower than baseline, and both LSP and LSPwC Type A. This suggests a decrease in oxygen reduction rate (ORR) for LSP samples with little to no residual stress, compared to baseline. In contrast, the ORR for LSP and LSPwC with intact residual stresses appear to have the same ORR as the baseline surface condition.

### Galvanostatic control

Figure 8(B) shows untreated AA7075 (baseline), LSP and LSPwC Type A and B under high galvanostatic control (2 h at  $2 \text{ mA cm}^{-2}$ ). LSP and LSPwC are either

within the baseline range or less than 50 mV from baseline. LSPwC shows a transient behaviour wherein the first 10–15 min, the potential is lower by 10–20 mV than baseline. From approximately 1 h into the galvanostatic control the potentials for all samples are within the baseline range, with some variation per sample (e.g. one LSPwC sample slightly higher by 20 mV).

Figure 8(C) shows a set of low galvanostatic control tests (all Type A), performed to view the change in potential for sample surfaces with a slower corrosion acceleration. The difference in potential values between baseline and LSP samples is less than 50 mV.

## Corrosion pit characterisation

### Corrosion pit initiation

Figure 9 shows typical AA7075-T651 corrosion pit initiation sites (after 72 h OCP) found on both baseline and LSP samples. In both cases trenching is evident adjacent to coarse intermetallics, due to microgalvanic coupling between the aluminium matrix and the coarse intermetallics, particularly  $\text{Al}_7\text{Cu}_2\text{Fe}$ . Additionally, from microscopy observation, there is no indication of a reduction in size or population of intermetallics at the surface, suggesting laser peening has not had an effect on these particles acting as efficient local cathodes and corrosion pit initiation sites.

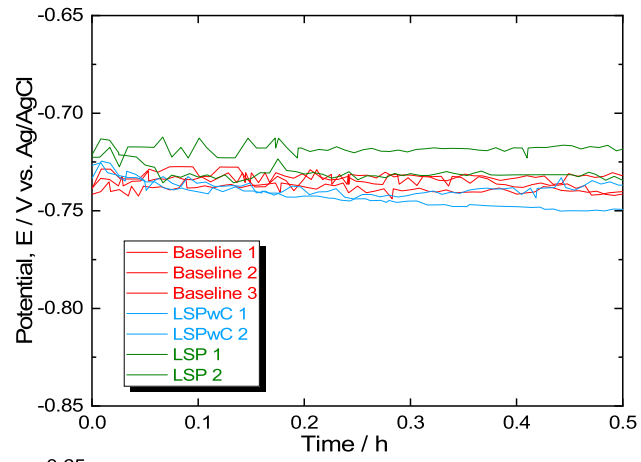
### Pit topography

Figure 10 provides representative topographical maps for the baseline, LSPwC samples before and after galvanostatic control (low). It is evident for all cases there are numerous pits 10–20  $\mu\text{m}$  in depth. Visual inspection suggests LSPwC has more corrosion pits than the baseline. In addition, it suggests LSPwC may have more corroded areas than baseline. This is similarly seen for LSP. It is important to note LSPwC and LSP samples already have some small pits, or depressions, present before corrosion exposure. These are assumed to be mechanical pits or generated during the laser-peening surface treatment or other surface features.

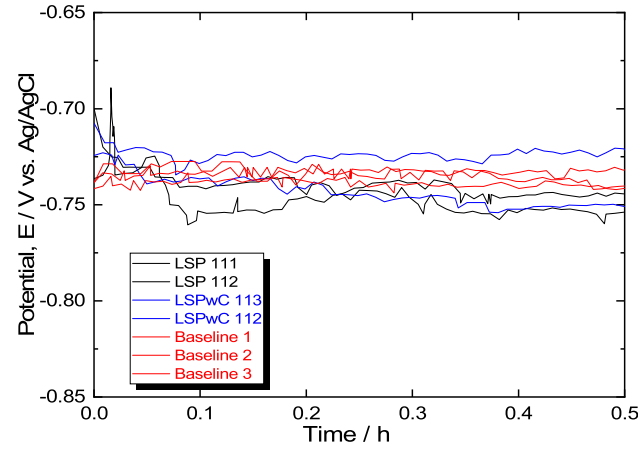
The pit density (number of pits per  $\text{mm}^2$ ), and the corroded area divided by the total projected area (pit area fraction) captured using the topographical images were assessed quantitatively, see Figure 11. Although there is some variation within each sample type (baseline, LSP or LSPwC), overall the LSP and LSPwC Type A show equivalent (high) or worse (low exposure) values to baseline. Type B show they are all similar to untreated AA7075 (baseline).

SEM imaging of corrosion pit cross-sections generated by galvanostatic control (Figure 12) show, as expected, pit depths are deeper than that assessed via topographical imaging. In all cases, irrespective of whether they are baseline or laser peened, the depth of pits is near 50  $\mu\text{m}$ , despite surface topography imaging showing pits of 10–30  $\mu\text{m}$  deep.

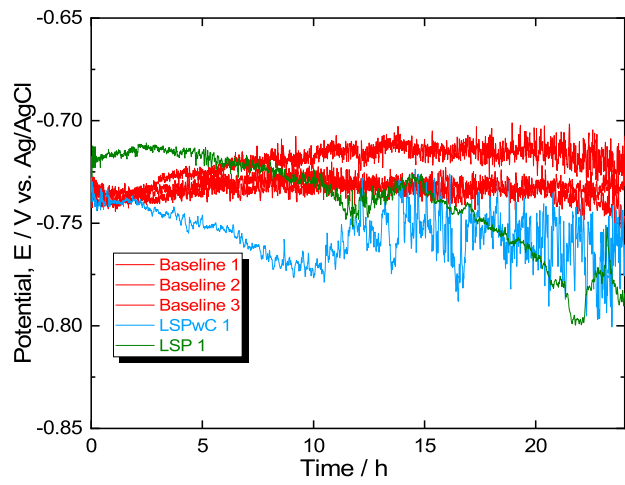
A: Type A - 30 mins



B: Type B - 30 mins



C: Type A - 24 h



D: Type B - 24 h

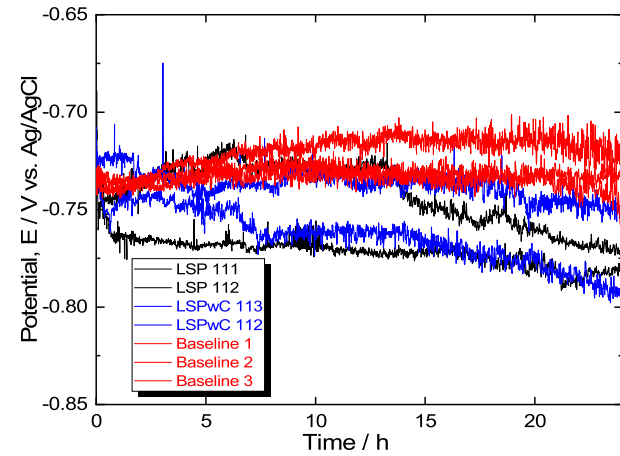


**Figure 7.** Open-circuit potential 30 min (A,B) and 24 h (C,D) for untreated AA7075 (baseline), LSP and LSPwC Type A and B samples.

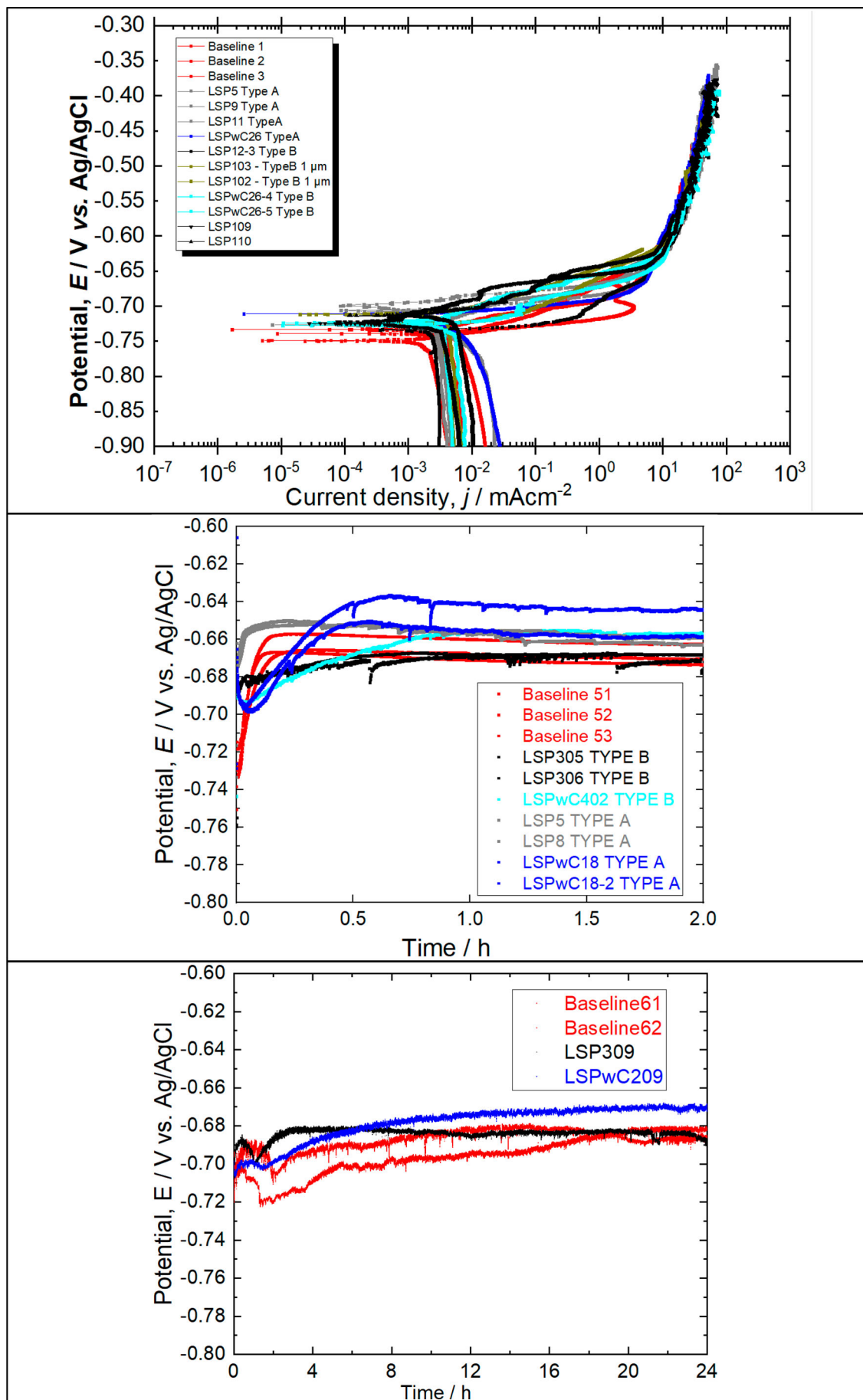


**Figure 8.** (A) Potentiodynamic polarisation of untreated AA7075 (baseline), LSP and LSPwC Type A and B. (B) High galvanostatic control (2 h) for the baseline, LSP, and LSPwC Type A and B samples. (C) Low galvanostatic control (24 h) for the baseline, LSP and LSPwC Type A.

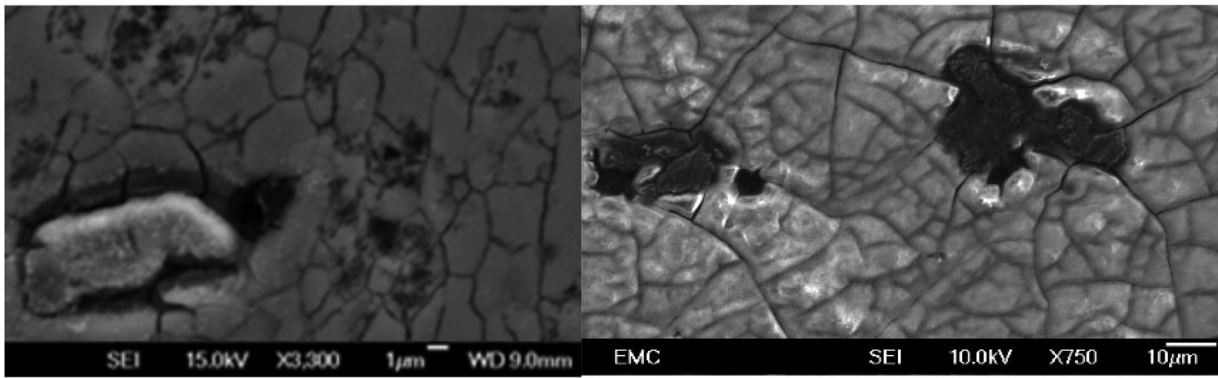


**Figure 9.** Pit initiation site at coarse constituent particles. Dissolution of aluminium alloy around cathodic particle due microgalvanic coupling. Left: untreated AA7075 (baseline). Right: LSP treated. All intermetallics in these images are  $Al_7Cu_2Fe$ .

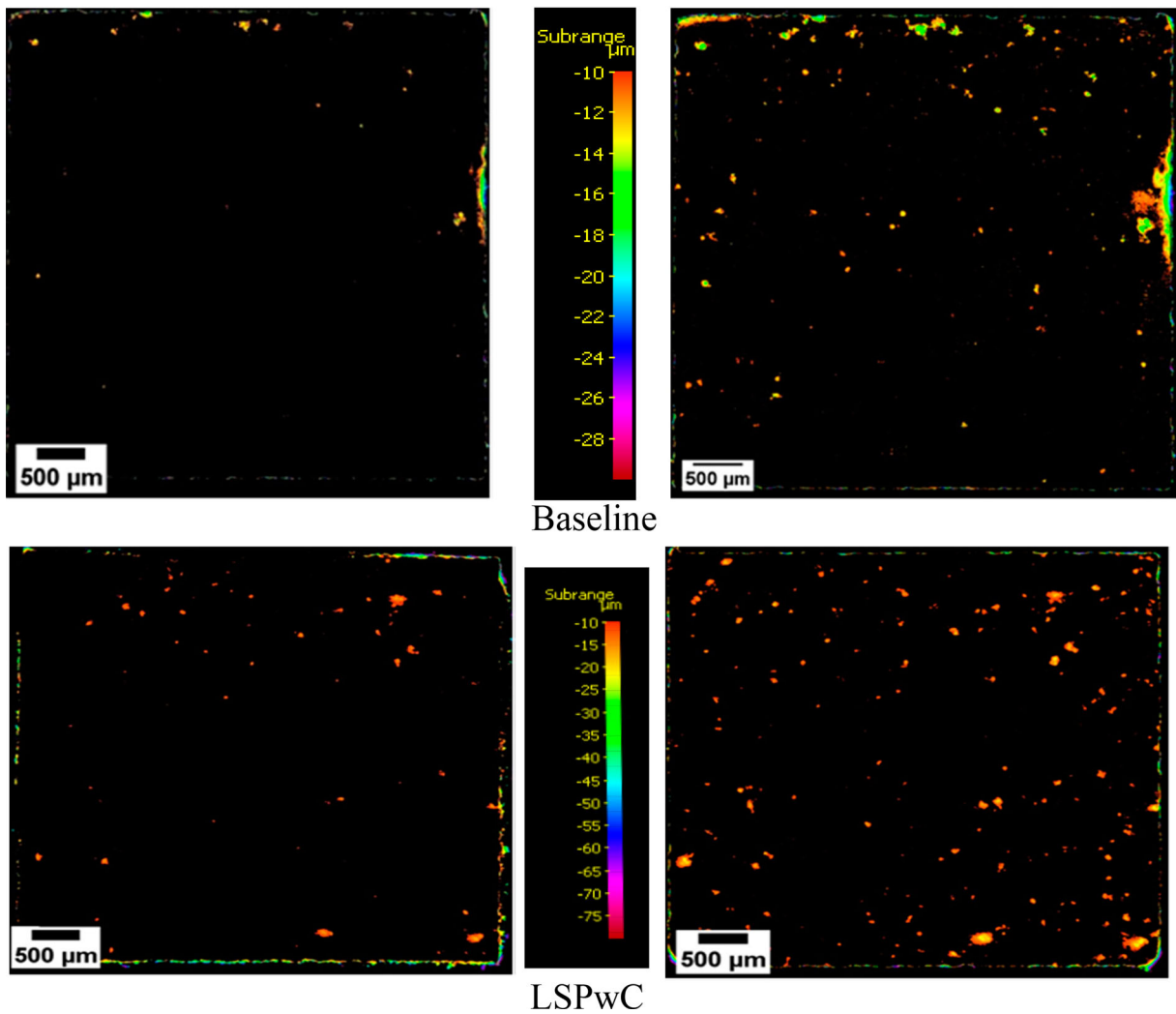


**Figure 10.** Surface profilometry of the AA7075 (baseline) and LSPwC surfaces after 24 h galvanostatic control at  $0.167 \text{ mA cm}^{-2}$ .

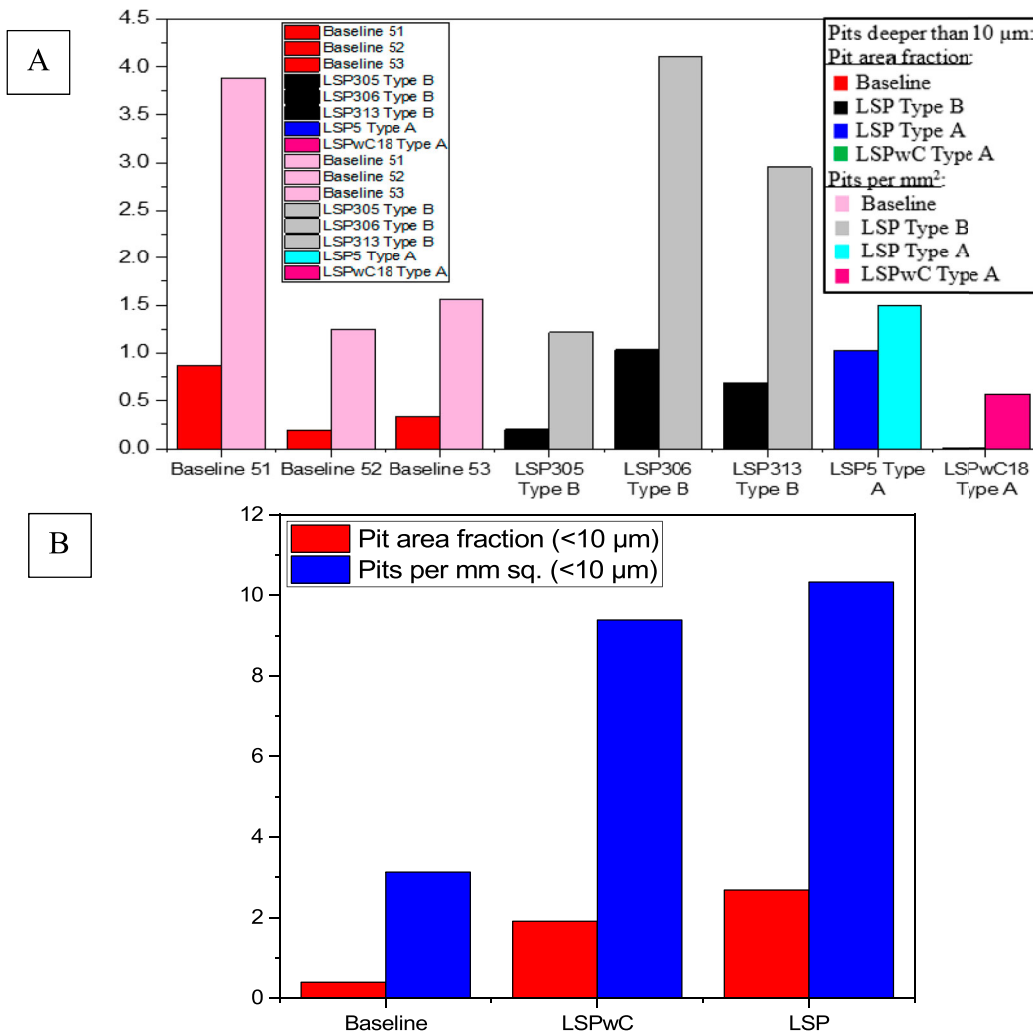
### Fatigue performance of pre-corroded surfaces

Figure 13 presents a typical example of a pre-corroded Type A sample before and after fatigue testing. According to the topographical examination, fatigue cracks do not necessarily initiate at the biggest or deepest pit. This is the case for AA7075 (baseline), LSP and LSPwC samples.

Figure 14 shows the baseline (untreated and uncorroded) AA7075 as-received ( $R_t = 2.64 \mu\text{m}$ ) and  $1 \mu\text{m}$

polished ( $R_t = 0.25 \mu\text{m}$ ) fatigue life which are quite similar. In contrast, baseline fatigue life decreased by at least 50% in the presence of pre-corroded pits. The crack propagation (Figure 15) is at the top of the baseline trend, suggesting it occurs slightly faster than for the uncorroded untreated AA7075 baseline surface condition. Figure 16 shows crack initiation occurs almost immediately and at least 95% of fatigue life is spent in crack propagation. The pre-corroded





**Figure 11.** Pit area fraction and pit density. Areas equal or bigger than 10 μm depth are considered corroded. (A) Baseline, LSP and LSPwC Type A and B samples galvanostatic control (2 h, 2 mA cm<sup>-2</sup>). (B) Baseline, LSPwC and LSP Type A samples only (24 h, 0.167 mA cm<sup>-2</sup>).

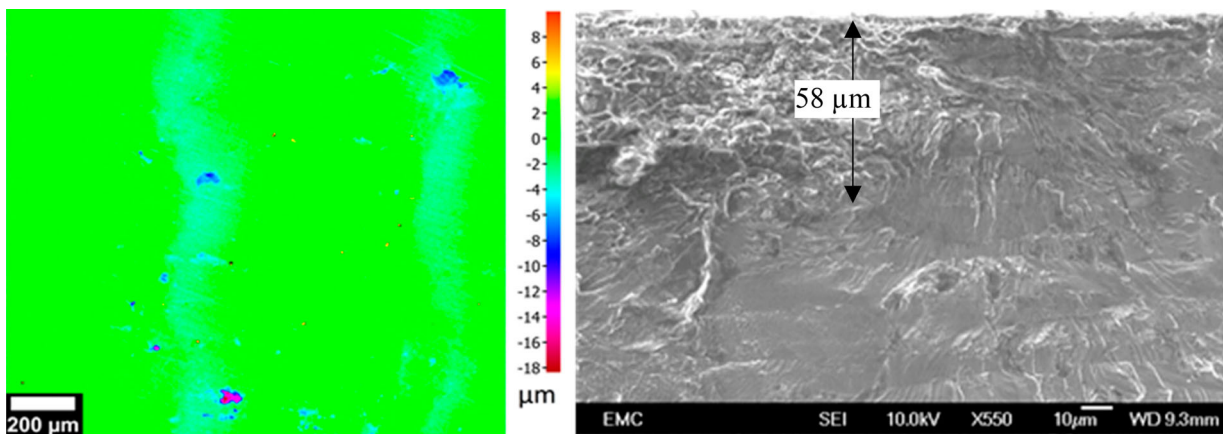


**Figure 12.** Left: Variable focus optical microscopy of pre-corroded LSP Type A sample. Right: SEM cross-section of pre-corroded pit feature in LSP sample showing true pit depth.

LSP and LSPwC are subject to an order of magnitude decrease in fatigue life when compared to their uncorroded condition: from millions of cycles to hundreds of thousands. Nevertheless, both LSP treatments have a better fatigue performance than the untreated AA7075 baseline (either pre-corroded or uncorroded).

Crack propagation data, although limited, shows a clear decrease in crack propagation rate for LSPwC compared to the baseline. For LSP, the crack propagation trendline lies near the bottom of the baseline trend, and considerably lower than the pre-corroded baseline samples. Crack initiation in both LSP and LSPwC

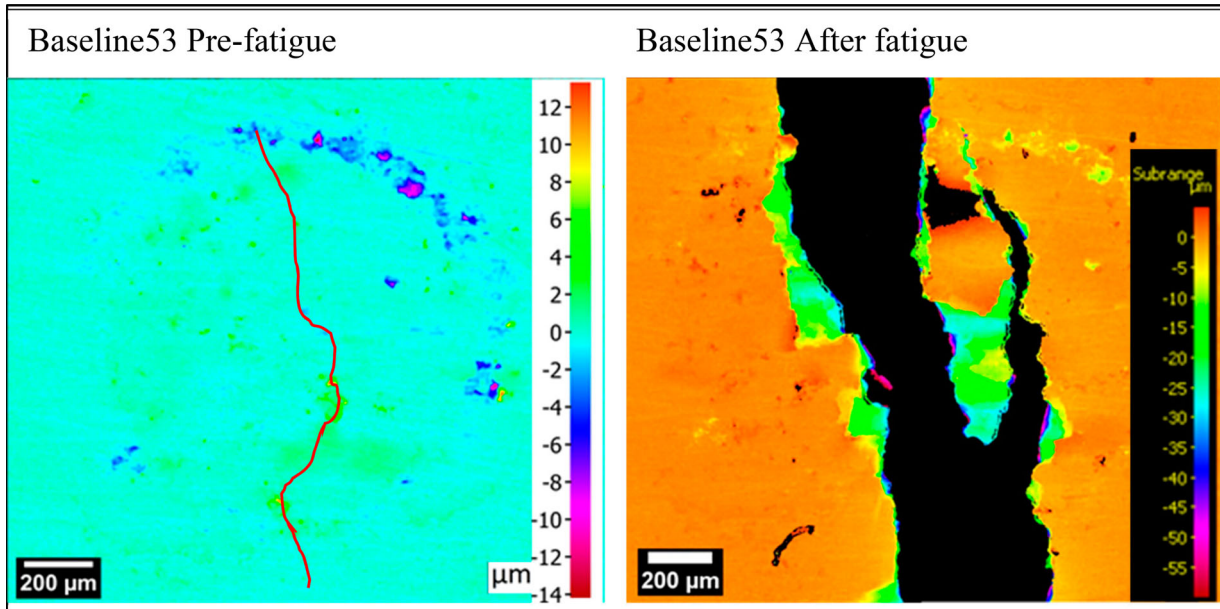


**Figure 13.** Variable focus optical microscopy of pre-corroded Type A sample before (left) and after (right) fatigue. Approximate fracture line is drawn in red.

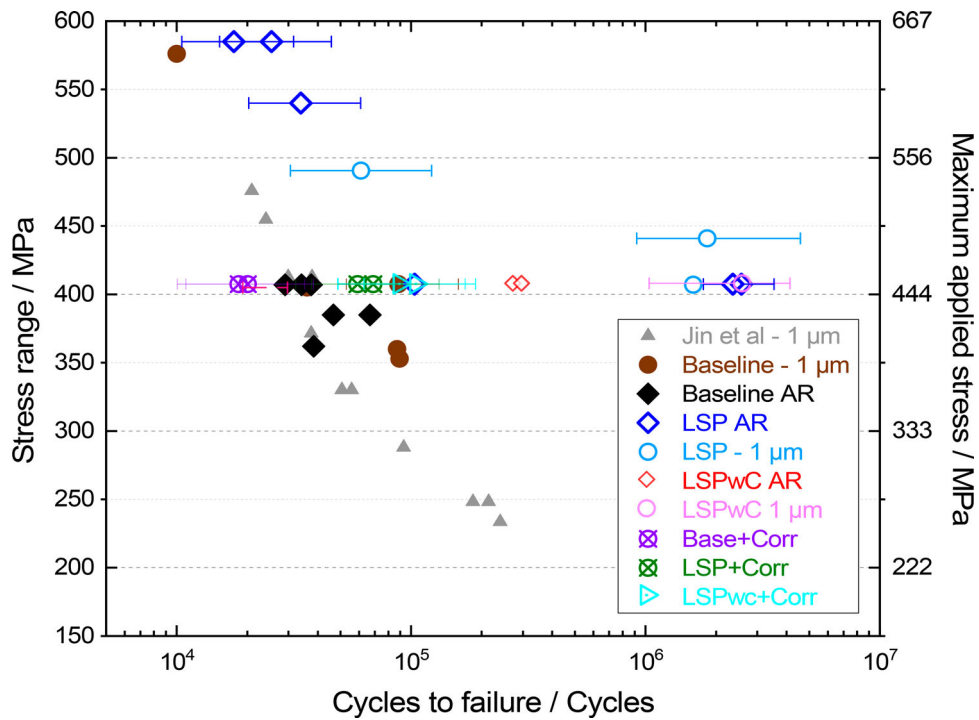


**Figure 14.** Stress range vs. cycles to failure for AA7075 Type A (baseline), LSP and LSPwC samples (pre-corroded and uncorroded). Uncorroded baseline and LSP samples are taken from Sanchez et al.

lasts for 30% of the total fatigue life, thus considerably increasing the fatigue initiation time: from near zero cycles in pre-corroded baseline to approximately 40,000 cycles in pre-corroded LSP. For crack propagation, life is increased from 40,000 in corroded baseline to 80,000 for LSP and 160,000 for LSPwC. This suggests a considerable delay in both crack initiation and propagation due to LSP-generated residual stresses.

## Discussion

### LSP surface and microstructural changes

Laser peening of AA7075 is a complex phenomenon, which produces irreversible interfacial changes leading to the generation of surface micro-heterogeneities (peened ripple topography linked to plastic deformation) and near-surface changes in the polycrystalline microstructure/misorientation. Factors such as residual

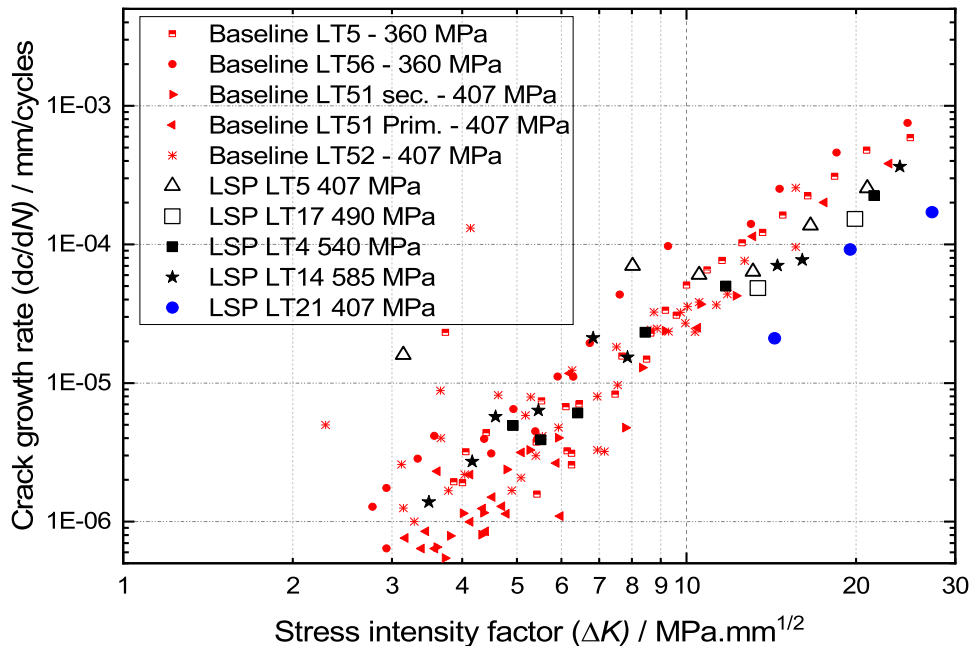


**Figure 15.** Crack growth ( $dc/dN$ ) vs. stress intensity factor range ( $\Delta K$ ) for baseline, LSP and LSPwC samples (pre-corroded and uncorroded). Baseline and LSP uncorroded samples are taken from Sanchez et al.

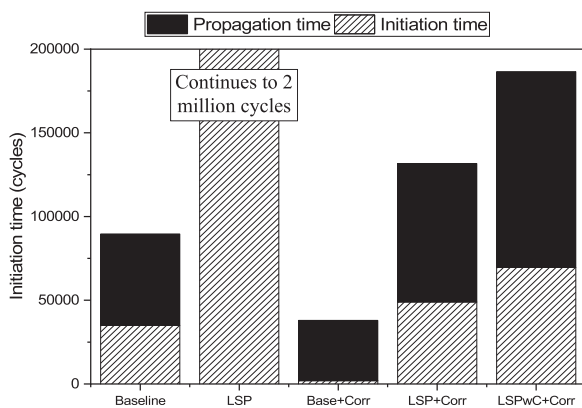


**Figure 16.** Average initiation and propagation life of untreated AA7075 (baseline), LSP (LSPwC is expected to be the same), pre-corroded baseline, pre-corroded LSP and pre-corroded LSPwC. Columns show total fatigue life, including cycles at 0.1 and 0.5 load ratio.

stress and roughness lead to a complex interplay of performance when these LSP-modified surfaces are subject to corrosion and fatigue environments.

As reported previously [24], residual stresses in LSP are higher or equal to previous laser-peening- or shot-peening-generated residual stresses in 7XXX alloys [11,20,23,25,26,30,38,43,54–57]. Figure 3 shows the LSPwC residual stresses within the initial 1 mm subsurface depth are up to 14% higher than for LSP. Thus, LSPwC also has higher residual stresses than previously reported in 7XXX alloys. The exception is at the surface, which is attributed to the LSPwC oxide layer formation and/or surface melting leading to weak residual stress generation ( $-85$  MPa). The subsequent mechanical polish partly resolves this surface issue but

ultimately does not achieve the higher magnitude residual stresses obtained by LSP with an ablative layer. Figure 6 [24] shows how the LSP KAM, and therefore plastic deformation, progressively decreases below the surface to considerably lower values: from near  $2^\circ$  at the surface to  $0.75^\circ$  at 1 mm below the surface, where minimal plastic deformation is anticipated. As such, relatively high levels of plastic deformation are concentrated near-surface for LSP, and the same would be expected of LSPwC.

Previous studies [58–61] have shown a clear link between hardness and residual stress. Small errors in the measurement of indent size in materials under compressive load (applied or residual) can lead to hardness overestimation, due to the residual stress effects on material pile-up at hardness indent edges. Thus, it is likely the apparent LSP hardness increase seen in this study (from 170 to 188 Hv) is in large part due to compressive residual stresses rather than the LSP-modified microstructure. When most residual stresses were removed (Type B), the hardness average decreased (175 Hv), although they were still slightly higher than for the untreated AA7075 (baseline). Considering LSPwC had similar peening parameters and residual stresses it would be expected to have similar hardness values to LSP. Instead, the LSPwC average and median hardness are only marginally higher than baseline. However, the variation in both Type A and B LSPwC samples is very large, particularly compared to baseline and LSP. It is likely there is an issue with testing accuracy due to higher roughness, and profile waviness, in LSPwC, as seen in Figure 5. Both the nature of non-ablative laser peening (ablation of alloy surface) and the subsequent mechanical polish to remove the

subsequent oxide layer, lead to this increased roughness and waviness profile. Although this roughness is mostly within the same magnitude as baseline, it is four times higher (for  $R_z$  and  $R_t$ ). Thus, a combination of the aforementioned indent pile-up effect and the surface/area ratio caused by roughness may be causing high variability in micro-hardness testing accuracy in LSPwC.

### **LSP effects on electrochemical and corrosion performance**

The short-term OCP results agree with similar studies for AA6082 LSPwC by Trdan and Grum [41,42], where small potential changes are seen after peening (below 50 mV) within the first hour. However, the long-term (24 h) OCP shows relatively stable potentials for untreated AA7075 baseline, whereas potentials for all the LSP and LSPwC (A or B) decreased suggesting the modified surface (specifically roughness) may be detrimental in the longer term. Laser peening having a negative effect on corrosion is not universal: e.g. Trdan and Grum [42] found a favourable decrease in the current density of AA6082 LSPwC during polarisation tests. Other studies see minor corrosion potential increases without changes in kinetic behaviour for AA6082 LSPwC [42,62] and low-plasticity burnished AA2024-T3 [63]. In terms of kinetic behaviour, the potentiodynamic polarisations in this study (Figure 8) appear to be consistent with the open-literature: small increases in the corrosion potential (below 50 mV) of laser-peened material and similar kinetic behaviour for untreated and laser-peened material: No significant difference is found between the baseline and laser-peened (Type A or B) anodic and cathodic branches. Although there is a variation for all types of tested conditions, the kinetic behaviours of LSP and LSPwC are within the baseline range. This agrees with results from other electrochemical tests of this study: Overall it suggests no conclusive significant differences in behaviour between untreated and laser shock peened or between type A and B samples. Fundamentally, the LSP compressive residual stress will affect the thermodynamics of these electrochemical active surfaces, i.e. the 'free-energy state' which may promote the formation of oxide layers, and these may be the cause of the slight raised free corrosion potential of laser-peened samples. The residual stress, plastic deformation and surface roughness will generally alter the corrosion either from enhanced cathodic kinetics, increased anodic dissolution (more initiation sites with increased surface activity) or via the formation of oxide layers (here subject to a compressive stress field). Overall, the combination of these conditions has not shown a conclusive kinetic effect on AA7075-T651. However, although the precise effect of laser-peening-induced surface roughness on AA7075-T651 corrosion is unclear, the only real conclusion that

can be drawn is that roughness could affect the electrochemical potential long-term.

When galvanostatically controlled (Figure 10), while there is no evidence of substantive corrosion, there are initially small transient differences, but subsequent pit characterisation shows no influence on pit density, pit size or depth for either LSP- or LSPwC-treated surface conditions. This is also different from that reported by Trdan and Grum [42,62], where a decrease in pit number and size was attributed to LSPwC surface melting changing the oxide layer ( $Al_2O_3$ ) and residual stresses. Melting of aluminium surfaces using lasers has been shown to generate a more homogeneous surface, with fewer second-phase particles [64,65], and to generate an oxide layer [42,65,66]. For the present study, the LSP (due to the ablative layer) and LSPwC (due to the subsequent mechanical polish removing any shallow melted layer that may be present) are unlikely to have this laser-induced oxide layer. This difference in the oxide layer may explain why there is no enhanced corrosion performance as seen in other LSPwC studies [41,42,62,66]. Thus, the small transient improvements in corrosion potential seen in this study could be attributed to compressive residual stresses, as this is not seen only in laser peened [41,42,62,66] but also in shot-peened [43] and low-plasticity burnished [63] aluminium alloys. It is also likely that the laser-peening-induced roughness, particularly LSPwC, counteracts the residual stress benefits. Zagar and Grum [43] show that LSP treatment led to surface roughness that promoted higher corrosion current densities, counteracting any possible LSP benefits. Figure 11, showing the high galvanostatic control, suggests this is the case: LSP Type B (reduced or no residual stresses) shows higher pit area fraction and pit density compared to the Type A condition, where residual stresses may be counteracting the detrimental effects of roughness. In contrast, the low (less aggressive) galvanostatic control shows a significant difference between baseline and laser-peened Type A. In this instance, laser peened may have performed worse due to the slower kinetics allowing roughness to play a more dominant role. This corroborates the 24 h OCP data, suggesting in long-term, natural (non-aggressive) exposure, roughness plays a significant role in pit corrosion development, being more dominant than any beneficial residual stress effects. In addition, although grain refinement was not captured quantitatively, it is known that changes in grain size can have an effect on corrosion performance [67]. However, the lack of conclusive evidence of changes in corrosion performance in this study suggests the expected grain refinement from both LSP and LSPwC has had a negligible effect in corrosion behaviour. Overall, this indicates surface roughness may be the most important variable in terms of electrochemical behaviour and corrosion performance after laser peening, offsetting any residual stress effects. For LSPwC, if the oxide layer is not removed it may also



provide an enhanced barrier to corrosion but this could not be evaluated in this study.

### **Mechanisms for AA7075-T651 corrosion initiation**

From Figure 9 it is evident there is no discernible change in pit corrosion mechanism after LSP, which is also seen for LSPwC. This agrees with the negligible minor effects seen in electrochemical behaviour after both laser-peening types. Aside from a few studies [41–43,62,66], residual stresses are reported to mostly have a significant effect only when retarding corrosion in processes where there is an external mechanical stimuli, such as corrosion fatigue and stress corrosion cracking [28–40]. In contrast, Liu and Frankel [63] evaluated the direction of compressive residual stress relative to the direction of intergranular corrosion (IGC). They observed compressive stresses (applied or residual) normal to the direction of preferred IGC (L-LT) reduced corrosion rates by closing intergranular sites. However, this benefit was not seen if the compressive stresses were parallel to the IGC direction. Unlike the Frankel study [63], the compressive residual stresses in this study are expected to be mainly parallel to the electrochemically exposed L-LT surface and as such the benefits of compression on IGC were not seen. Thus, for this study, the dominant role of second-phase intermetallics in corrosion pit initiation and growth, which is well documented [68,69], and the role of IGC, were clearly unchanged by the laser-peening-induced residual stresses or the modified surface. Future work should study similar electrochemical tests on AA7075-T651 with LSP treatment, and thus compressive residual stresses, normal to the preferred direction of IGC (L-LT plane), and likewise, to investigate LSPwC without removing its generated oxide layer. This oxide layer and the resulting homogenised surface caused by laser melting may change the overall electrochemical behaviour, giving a small to moderate improvement in electrochemical properties and reduce the number and size of pits.

### **LSP effects on fatigue behaviour of pre-corroded AA7075-T651**

Evaluation of the fractured fatigue samples (Figure 12) showed cracks do not necessarily initiate at the deepest or widest pits within a pre-corroded surface. In several cases, cracks originated at what appear to be 10- $\mu$ m-deep pits. SEM microscopy of pit cross-sections shows many of these apparently discrete pits are in fact connected to one another below the surface. Thus, the pit morphology under the surface is more complex. Cracks initiate subsurface and at the sharp edges of these complex pits, where the stress concentration is highest.

Fatigue S-N data (Figure 14), and microscopy of beach-marked fracture surfaces reveal the decrease in fatigue life of corroded baseline samples is due to a near-complete absence of crack initiation time. This confirms pits (mechanical or corrosion), act as effective stress concentrations, initiating cracks shortly after dynamic loading starts. The crack growth rate vs. stress intensity factor ( $\Delta K$ ) data in Figure 15 suggest that the crack growth rate of corroded baseline is not particularly faster than uncorroded baseline, although it sits on the upper limits of this data trend. This may be due to all samples having at least two cracks initiating close together and coalescing shortly after. Thus, crack growth rates are marginally faster than uncorroded baseline due to multi-site cracking. This, and the fact the cracks already start 50  $\mu$ m below the surface (at pits) may explain why crack growth life is lower than for uncorroded baseline.

Pre-corroded LSP S-N and crack growth rate vs.  $\Delta K$  data show compressive residual stresses delay crack initiation by effectively counteracting stress concentrations at pits. The higher compressive residual stresses in corroded LSPwC samples means crack initiation and crack propagation are delayed more effectively than corroded LSP, as seen in Figure 15. It is likely residual stresses are playing a part in delaying crack propagation of small cracks ( $\Delta K \leq 10$ ); however, multi-site fatigue crack growth likely accelerates the overall crack growth rate. The overall increase in fatigue life is +250% and 400% for LSP and LSPwC, respectively. Zupanc and Grum reported a similar improvement (an order of magnitude increase) in fatigue performance [36] in shot-peened AA7075. Thus the fatigue life improvement from the corroded surfaces is not due to laser peening changing the mechanism of fatigue crack initiation in pits. Instead, the improvement in fatigue life is solely connected to the level of residual stresses, and how effectively they delay crack initiation and propagation.

### **Conclusions**

Laser shock peening with and without an ablative coating (LSP and LSPwC) generated deep compressive residual stress fields of up to  $-400$  MPa in AA7075-T651, whilst also causing a small increase in surface roughness for LSP, and a moderate increase for LSPwC. Additionally, laser peening caused a small increase (up to 11%) in surface hardness for LSP and likely for LSPwC. Key study insights include:

- There is no conclusive evidence of long-term effects of compressive residual stresses on corrosion performance, changes in the corrosion pit initiation mechanism, or the number or depth of pits, for the LSP and LSPwC treated AA7075-T651, where no external mechanical stimulus is involved. This may not be

the case if compressive residual stresses are normal to the direction of preferred intergranular corrosion, and this should be investigated further.

- Laser-shock-peening-induced surface roughness can be a dominant feature and be detrimental to long-term corrosion performance. The LSPwC-induced oxide layer, not covered in this study, could be beneficial to corrosion performance and this should be investigated further in conjunction with its fatigue performance.
- Corrosion pits in untreated AA7075-T651 act as stress concentrations causing at least a 50% loss in fatigue life, mainly due to a near-complete absence of crack initiation time. Laser-shock-peen-generated residual stresses effectively counteract stress concentrations at pits, substantially delaying crack initiation by at least 40,000 cycles. The residual stresses also delay crack propagation, with LSPwC (160,000 cycles) performing better than LSP (80,000 cycles) due to the higher compressive residual stresses. Overall, laser-peened AA7075-T651 with corrosion pit degradation can be expected to have a fatigue performance and a lifetime equivalent or better than uncorroded unpeened AA7075-T651.

### Disclosure statement

No potential conflict of interest was reported by the author(s).

### Funding

This study is financially supported by the Engineering and Physical Sciences Research Council (EPSRC), UK [grant number EP/N509747/1]. The authors would like to acknowledge the funding and support of the University of Southampton. Michael E. Fitzpatrick is grateful for funding from the Lloyd's Register Foundation, a charitable foundation helping protect life and property by supporting engineering-related education, public engagement, and the application of research.

### Data availability statement

The raw data required to reproduce these findings are available to download from the University of Southampton repository at <https://doi.org/10.5258/SOTON/D1949>. The processed data required to reproduce these findings are available to download from <https://doi.org/10.5258/SOTON/D1949>.

### Nomenclature and abbreviations

7XXX	Seven thousand series aluminium alloys
BEI	Backscatter electron imaging
CSIR	Council for Scientific and Industrial Research
EBSD	Electron backscatter diffraction
EDS	Energy-dispersive spectroscopy
IGC	Intergranular corrosion

KAM	Kernel average misorientation
L	Longitudinal microstructural direction
LSP	Ablative laser shock peening
LSPwC	Non-ablative laser shock peening (Laser peening without coating)
LT	Long transverse microstructural direction
NaCl	Sodium chloride
OCP	Open-circuit potential
ORR	Oxygen reduction rate
SEI	Secondary electron imaging
SEM	Scanning electron microscope
SiC	Silicon carbon grit paper
ST	Short transverse microstructural direction
XRD	X-ray diffraction

### Terminology

$\Delta K$	Stress intensity factor range
$da/dN$	Crack growth vs. number of cycles
$E$	Potential
$E_{\text{corr}}$	Corrosion potential
$h$	hours
Hv	Vickers hardness
$j$	current density
keV	Electronvolt
kg-f	kilogram force
$R_a$	Mean roughness
$R_q$	Root mean square roughness
$R_{\text{sk}}$	Skewness
$R_t$	Maximum roughness depth
$R_z$	Mean roughness depth
$s$	seconds
$S_1$	Compressive residual stress measurement direction parallel to L
$S_3$	Compressive residual stress measurement direction parallel to LT
$N_{R=0.1}$	Number of fatigue cycles in 0.1 load ratio
$N_{R=0.5}$	Number of fatigue cycles in 0.5 load ratio
$N_{\text{Total}}$	Total number of fatigue cycles based on Equation (1)

### ORCID

A. G. Sanchez  <http://orcid.org/0000-0002-7246-7000>

M. E. Fitzpatrick  <http://orcid.org/0000-0002-3618-6594>

### References

- [1] Luo K, Lu J, Zhang L, et al. The microstructural mechanism for mechanical property of LY2 aluminum alloy after laser shock processing. *Mater Des.* 2010 May 1;31(5):2599–2603.
- [2] Lu JZ, Luo KY, Zhang YK, et al. Grain refinement of LY2 aluminum alloy induced by ultra-high plastic strain during multiple laser shock processing impacts. *Acta Mater.* 2010 Jun 1;58(11):3984–3994.
- [3] Ding K, Ye L. General introduction. In: Laser shock peening. Elsevier; 2006. p. 1–6. [Internet]. [cited 2020

- Feb 6] Available from: <https://linkinghub.elsevier.com/retrieve/pii/B9781855739291500019>
- [4] Fairand BP, Clauer AH. Applications of laser-induced stress waves. In: Lasers in modern industry seminar. Cambridge (MA): Society of Manufacturing Engineers; 1978. [Internet]. [cited 2018 Jun 24]. Available from: <https://www.lsptechnologies.com/wp-content/uploads/2008/05/pub1007.pdf>
  - [5] Clauer AH, Holbrook JH, Fairand BP. Effects of laser induced shock waves on metals. In: Meyers MA, Murr LE, editors. Shock waves and high-strain-rate phenomena in metals. New York: Plenum; 1981. p. 676–703. [Internet]. [cited 2018 Jun 18]. Available from: [https://pdfs.semanticscholar.org/455d/801567d88a167df85a2bc56bae6384c0d345.pdf?\\_ga=2.12254772.1275154946.1529304832-1115821980.1529304832](https://pdfs.semanticscholar.org/455d/801567d88a167df85a2bc56bae6384c0d345.pdf?_ga=2.12254772.1275154946.1529304832-1115821980.1529304832)
  - [6] Sano Y, Akita K, Masaki K, et al. Laser peening without coating as a surface enhancement technology. *J Laser Micro/Nanoeng.* 2006;1(3):161–166.
  - [7] Clauer AH. Laser shock peening for fatigue resistance. *Surf Perform Titan.* 1996;217:230.
  - [8] Peyre P, Fabbro R, Berthe L, et al. Laser shock processing of materials, physical processes involved and examples of applications. *J Laser Appl.* 1996;8(3):135–141.
  - [9] Becker A. The effect of laser shock peening and shot peening on the fatigue performance of aluminium alloy 7075. Cape Town: University of Cape Town; 2017.
  - [10] Gao YK. Improvement of fatigue property in 7050–T7451 aluminum alloy by laser peening and shot peening. *Mater Sci Eng A.* 2011 Apr 25;528(10–11):3823–3828. [Internet]. [cited 2018 Oct 25]. Available from: <https://www.sciencedirect.com/science/article/pii/S0921509311000992>
  - [11] Peyre P, Fabbro R, Merrien P, et al. Laser shock processing of aluminium alloys. Application to high cycle fatigue behaviour. *Mater Sci Eng A.* 1996 Jun 15;210(1–2):102–113. [Internet]. [cited 2018 Oct 25]. Available from: <https://www.sciencedirect.com/science/article/pii/S0921509395100849>
  - [12] Dorman M, Toparli MB, Smyth N, et al. Effect of laser shock peening on residual stress and fatigue life of clad 2024 aluminium sheet containing scribe defects. *Mater Sci Eng A.* 2012 Jun 30;548:142–151.
  - [13] Clauer AH, Walters CT, Ford SC. The effects of laser shock processing on the fatigue properties of 2024-T3 aluminum. *ASM Conference on Lasers in Materials Processing*; Los Angeles; 1986. p. 7–22. [Internet]. [cited 2020 Apr 3]. Available from: [https://www.researchgate.net/publication/283967984\\_The\\_Effects\\_of\\_Laser\\_Shock\\_Processing\\_on\\_the\\_Fatigue\\_Properties\\_of\\_2024-T3\\_Aluminum](https://www.researchgate.net/publication/283967984_The_Effects_of_Laser_Shock_Processing_on_the_Fatigue_Properties_of_2024-T3_Aluminum)
  - [14] Zabeen S, Langer K, Fitzpatrick ME. Effect of alloy temper on surface modification of aluminium 2624 by laser shock peening. *Surf Coat Technol.* 2018;347(March):123–135.
  - [15] Abeens M, Muruganandhan R, Thirumavalavan K, et al. Surface modification of AA7075 T651 by laser shock peening to improve the wear characteristics. *Mater Res Express.* 2019 Mar 15;6(6):1–13.
  - [16] Liu Q. An effective life extension technology for 7xxx series aluminium alloys by laser shock peening. Victoria; 2008. [Internet]. [cited 2018 Nov 27]. Available from: <http://citeseerx.ist.psu.edu/viewdoc/download?doi=10.1.1.427.4977&rep=rep1&type=pdf>
  - [17] Liu Q, Barter S, Clark G. Internal cracking during surface treatment of 7050-T74 aluminium alloy using laser shock peening. *Struct. Integr. Fract. Proc. Int. Conf. SIF 2002*; Perth, Australia; 2002 Sep 25–28. 177.
  - [18] Carpio FJ, Araújo D, Pacheco FJ, et al. Fatigue behaviour of laser machined 2024 T3 aeronautic aluminium alloy. *Appl Surf Sci.* 2003 Mar 15;208–209(1):194–198.
  - [19] Grum J, Trdan U, Hill MR. Laser shock processing of ENAW 6082 aluminium alloy surface. *Mater Sci Forum.* 2008;589:379–384.
  - [20] Zhang XQQ, Li H, Yu XLL, et al. Investigation on effect of laser shock processing on fatigue crack initiation and its growth in aluminum alloy plate. *Mater Des.* 2015 Jan 1;65:425–431. [Internet]. [cited 2018 Oct 25]. Available from: <https://www.sciencedirect.com/science/article/pii/S0261306914006906>
  - [21] Gencalp Irizalp S, Saklakoglu N, Akman E, et al. Pulsed Nd: YAG laser shock processing effects on mechanical properties of 6061-T6 alloy. *Opt Laser Technol.* 2014 Mar 1;56:273–277.
  - [22] Trdan U, Ocaña JL, Grum J. Surface modification of aluminium alloys with laser shock processing. *J Mech Eng.* 2010;57(5):385–393. [Internet]. [cited 2020 Apr 4]. Available from: <https://www.researchgate.net/publication/259216981>
  - [23] Ivetic G, Meneghin I, Troiani E, et al. Characterisation of fatigue and crack propagation in laser shock peened open hole 7075-T73 aluminium specimens. *ICAF 2011 Structural Integrity: Influence of Efficiency and Green Imperatives – Proceedings of the 26th Symposium of the International Committee on Aeronautical Fatigue.* Dordrecht: Springer; 2011. p. 855–866.
  - [24] Sanchez AG, You C, Leering M, et al. Effects of laser shock peening on the mechanisms of fatigue short crack initiation and propagation of AA7075-T651. *Int J Fatigue.* 2021 Feb 1;143:106025. [Internet]. [cited 2020 Nov 10]. Available from: <https://linkinghub.elsevier.com/retrieve/pii/S0142112320305570>
  - [25] Luong H, Hill MR. The effects of laser peening and shot peening on high cycle fatigue in 7050-T7451 aluminum alloy. *Mater Sci Eng A.* 2010;527(3):699–707.
  - [26] Luong H, Hill MR. The effects of laser peening on high-cycle fatigue in 7085-T7651 aluminum alloy. *Mater Sci Eng A.* 2008;477(1–2):208–216.
  - [27] Research and Technology Organisation, North Atlantic Treaty Organisation. Corrosion fatigue and environmentally assisted cracking in aging military vehicles; 2011. [Internet]. Available from: <http://www.rto.nato.int/Pubs/rdp.asp?RDP=RTO-AG-AVT-140>
  - [28] Brandenburg KA, Hornbach DJ, Mason PW. Use of engineered compressive residual stresses to mitigate stress corrosion cracking and corrosion fatigue in sensitized 5XXX Series aluminum alloys. *Proceedings of Department of Defense Virtual Corrosion Conference*; Cincinnati; 2013. [Internet]. [cited 2020 Jul 31]. Available from: <https://www.lambdatechs.com/wp-content/uploads/287.pdf>
  - [29] Lu JZ, Luo KY, Yang DK, et al. Effects of laser peening on stress corrosion cracking (SCC) of ANSI 304 austenitic stainless steel. *Corros Sci.* 2012 Jul 1;60:145–152.
  - [30] Wang JT, Zhang YK, Chen JF, et al. Effects of laser shock peening on stress corrosion behavior of 7075 aluminum alloy laser welded joints. *Mater Sci Eng A.* 2015 Oct 28;647:7–14.
  - [31] Telang A, Gill AS, Teyseyre S, et al. Effects of laser shock peening on SCC behavior of alloy 600 in tetrathionate solution. *Corros Sci.* 2015 Jan 1;90:434–444.
  - [32] Yu J, Gou G, Zhang L, et al. Ultrasonic impact treatment to improve stress corrosion cracking resistance of



- welded joints of aluminum alloy. *J Mater Eng Perform.* 2016 Jul 1;25(7):3046–3056. [Internet]. [cited 2020 Sep 3]. Available from: <https://link.springer.com/article/10.1007/s11665-016-2087-3>
- [33] Sundar R, Ganesh P, Kumar BS, et al. Mitigation of stress corrosion cracking susceptibility of machined 304L stainless steel through laser peening. *J Mater Eng Perform.* 2016 Sep 1;25(9):3710–3724. [Internet]. [cited 2020 Sep 3]. Available from: <https://link.springer.com/article/10.1007/s11665-016-2220-3>
- [34] Hyatt MV. Effects of residual stresses on stress corrosion crack growth rates in aluminum alloy. *Corrosion.* 1970;26(12):547–551.
- [35] Hawkes GA. Effect of shot peening on stress-corrosion properties and stress distribution in aluminium alloy d.t.d. 5054. *Br Corros J.* 1968;3(5):258–261.
- [36] Zupanc U, Grum J. Effect of pitting corrosion on fatigue performance of shot-peened aluminium alloy 7075-T651. *J Mater Process Technol.* 2010 Jun 19;210(9):1197–1202. [Internet]. [cited 2018 Dec 12]. Available from: <https://www.sciencedirect.com/science/article/pii/S0924013610000774>
- [37] Luo KY, Yin YF, Wang CY, et al. Effects of laser shock peening with different coverage layers on fatigue behaviour and fractural morphology of Fe-Cr alloy in NaCl solution. *J Alloys Compd.* 2019 Jan 30;773:168–179.
- [38] Wang H, Ning C, Huang Y, et al. Improvement of abrasion resistance in artificial seawater and corrosion resistance in NaCl solution of 7075 aluminum alloy processed by laser shock peening. *Opt Lasers Eng.* 2017 Mar 1;90:179–185.
- [39] Abdulstaar M, Mhaede M, Wollmann M, et al. Investigating the effects of bulk and surface severe plastic deformation on the fatigue, corrosion behaviour and corrosion fatigue of AA5083. *Surf Coat Technol.* 2014 Sep 15;254:244–251. [Internet]. [cited 2018 Dec 13]. Available from: <https://www.sciencedirect.com/science/article/pii/S0257897214005374>
- [40] Zhao W, Liu D, Zhang X, et al. Improving the fretting and corrosion fatigue performance of 300M ultra-high strength steel using the ultrasonic surface rolling process. *Int J Fatigue.* 2019 Apr 1;121:30–38.
- [41] Trdan U, Grum J. Investigation of corrosion behaviour of aluminium alloy subjected to laser shock peening without a protective coating. *Adv Mater Sci Eng.* 2015;2015:9.
- [42] Trdan U, Grum J. Evaluation of corrosion resistance of AA6082-T651 aluminium alloy after laser shock peening by means of cyclic polarisation and EIS methods. *Corros Sci.* 2012;59:324–333.
- [43] Zagar S, Grum J. Roughness, residual stresses and pitting corrosion effect on shot peened AA 7075. *Tech Gazette.* 2015;22(6):1589–1595.
- [44] ASM Aerospace Specification Metals Inc. Aluminium 7075-T6. 7075-T651. *MatWeb*; 2001. [Internet]. [cited 2020 Jan 3]. Available from: <http://asm.matweb.com/search/SpecificMaterial.asp?bassnum=MA7075T6>
- [45] Schajer GS, editor. *Practical residual stress measurement methods.* 1st ed., Vol. 1. Vancouver: Wiley, University of Columbia; 2013. p. 1–12.
- [46] Niknam SA, Songmene V. Deburring and edge finishing of aluminum alloys: A review. *Proceedings of the 12th International Aluminum Conference (INALCO)*; Montreal; 2013. [Internet]. [cited 2020 Jun 18]. Available from: [https://www.researchgate.net/publication/263966600\\_Deburring\\_and\\_edge\\_finishing\\_of\\_aluminum\\_all\\_oys\\_A\\_review](https://www.researchgate.net/publication/263966600_Deburring_and_edge_finishing_of_aluminum_all_oys_A_review)
- [47] Bachmann F, Hielscher R, Schaeben H. Grain detection from 2d and 3d EBSD data-specification of the MTEX algorithm. *Ultramicroscopy.* 2011 Dec;111(12):1720–1733.
- [48] Grant PV, Lord JD, Whitehead PS. The measurement of residual stresses by the incremental hole drilling technique. *Meas Good Pract Guid.* 2006;53(2):63.
- [49] Schindelin J, Arganda-Carreras I, Frise E, et al. Fiji: an open-source platform for biological-image analysis. *Nat Methods.* 2012 Jul 1;9(7):676–682. [Internet]. [cited 2018 Oct 12]. Available from: <http://www.nature.com/articles/nmeth.2019>
- [50] Dowling NE, Calhoun CA, Arcari A. Mean stress effects in stress-life fatigue and the Walker equation. *Fatigue Fract Eng Mater Struct.* 2009 Mar;32(3):163–179. [Internet]. [cited 2020 Apr 13]. Available from: <http://doi.wiley.com/10.1111/j.1460-2695.2008.01322.x>
- [51] Zhao T, Jiang Y. Fatigue of 7075-T651 aluminum alloy. *Int J Fatigue.* 2008;30(5):834–849.
- [52] Humphreys FJ. Grain and subgrain characterisation by electron backscatter diffraction. *J Mater Sci.* 2001;36:3833–3854. [Internet]. [cited 2020 Oct 16]. Available from: <https://link.springer.com/article/10.1023/A:1017973432592>
- [53] Singh S, Guo Y, Winiarski B, et al. High resolution low kV EBSD of heavily deformed and nanocrystalline aluminium by dictionary-based indexing. *Sci Rep.* 2018 Dec 1;8(1):10991. [Internet]. [cited 2020 Oct 16]. Available from: [www.nature.com/scientificreports/](http://www.nature.com/scientificreports/)
- [54] Mhaede M, Sano Y, Altenberger I, et al. Fatigue performance of Al7075-T73 and Ti-6Al-4V: comparing results after shot peening. *Laser shock peening and ball-burnishing.* *Proc Shot Peen ICS.* 2011;11:2–7.
- [55] Wang JT, Zhang YK, Chen JE, et al. Effect of laser shock peening on the high-temperature fatigue performance of 7075 aluminum alloy. *Mater Sci Eng A.* 2017 Sep 17;704:459–468.
- [56] Zupanc U, Grum J. Surface integrity of shot peened aluminium alloy 7075-T651. *Stroj Vestn J Mech E.* 2011;57(5):379–384.
- [57] Pandey V, Singh JKK, Chattopadhyay K, et al. Influence of ultrasonic shot peening on corrosion behavior of 7075 aluminum alloy. *J Alloys Compd.* 2017 Nov 5;723:826–840. [Internet]. [cited 2018 Dec 11]. Available from: <https://www.sciencedirect.com/science/article/pii/S0925838817323186>
- [58] Simes TR, Mellor SG, Hills DA. A note on the influence of residual stress on measured hardness. *J Strain Anal Eng Des.* 1984 Apr 3;19(2):135–137. [Internet]. [cited 2020 Oct 12]. Available from: <http://journals.sagepub.com/doi/10.1243/03093247V192135>
- [59] Tsui TY, Oliver WC, Pharr GM. Influences of stress on the measurement of mechanical properties using nanoindentation: part I. experimental studies in an aluminum alloy. *J Mater Res.* 1996;11(3):752–759. [Internet]. [cited 2020 Oct 12]. Available from: [/core/journals/journal-of-materials-research/article/influences-of-stress-on-the-measurement-of-mechanical-properties-using-nanoindentation-part-i-experimental-studies-in-an-aluminum-alloy/8BE85EA25B83F079B68B7D3D2081D211](http://core/journals/journal-of-materials-research/article/influences-of-stress-on-the-measurement-of-mechanical-properties-using-nanoindentation-part-i-experimental-studies-in-an-aluminum-alloy/8BE85EA25B83F079B68B7D3D2081D211)
- [60] Khan MK, Fitzpatrick ME, Hainsworth SV, et al. Effect of residual stress on the nanoindentation response of aerospace aluminium alloys. *Comput Mater Sci.* 2011 Aug 1;50(10):2967–2976.



- [61] Khan MK, Fitzpatrick ME, Hainsworth SV, et al. Application of synchrotron X-ray diffraction and nanoindentation for the determination of residual stress fields around scratches. *Acta Mater.* 2011 Dec 1;59(20):7508–7520.
- [62] Trdan U, Grum J. SEM/EDS characterization of laser shock peening effect on localized corrosion of Al alloy in a near natural chloride environment. *Corros Sci.* 2014 May 1;82:328–338. [Internet]. [cited 2018 May 31]. Available from: <https://www.sciencedirect.com/science/article/pii/S0010938X1400047X>
- [63] Liu X, Frankel GS. Effects of compressive stress on localized corrosion in AA2024-T3. *Corros Sci.* 2006;48(10):3309–3329.
- [64] Elkandari BMHM. Excimer laser surface melting treatment on 7075-T6 aluminium alloy for improved corrosion resistance. University of Manchester; 2012. [Internet]. [cited 2018 Jun 6]. Available from: <https://www.escholar.manchester.ac.uk/api/datastream?publicationPid=uk-ac-man-scw:189196&datastreamId=FULL-TEXT.PDF>
- [65] Chan CP, Yue TM, Man HC. The effect of excimer laser surface treatment on the pitting corrosion fatigue behaviour of aluminium alloy 7075. *J Mater Sci.* 2003 Jul 15;38(12):2689–2702. [Internet]. [cited 2020 Oct 28]. Available from: <https://link.springer.com/article/10.1023/A:1024498922104>
- [66] Pariona MM, Teleginski V, Dos Santos K, et al. AFM study of the effects of laser surface remelting on the morphology of Al-Fe aerospace alloys. *Mater Charact.* 2012 Dec 1;74:64–76.
- [67] Ralston KD, Fabijanic D, Birbilis N. Effect of grain size on corrosion of high purity aluminium. *Electrochim Acta.* 2011 Jan;56(4):1729–1736. [Internet]. Available from: <https://linkinghub.elsevier.com/retrieve/pii/S0013468610011837>
- [68] Birbilis N, Cavanaugh MK, Buchheit RG. Electrochemical behavior and localized corrosion associated with Al<sub>7</sub>Cu<sub>2</sub>Fe particles in aluminum alloy 7075-T651. *Corros Sci.* 2006;48(12):4202–4215.
- [69] Birbilis N, Buchheit RG. Electrochemical characteristics of intermetallic phases in aluminum alloys. *J Electrochem Soc.* 2005;152(4):B140. [Internet]. [cited 2017 Jun 20]. Available from: <http://jes.ecsdl.org/cgi/doi/10.1149/1.1869984>